

Geochemistry, Geophysics, Geosystems

RESEARCH ARTICLE

10.1029/2019GC008182

Key Points:

- Late Eocene accelerated deepening of the Tasman Gateway led to invigorated surface and bottom water circulation in the Southern Ocean
- Biomarker paleothermometry and quantitative dinocyst distribution patterns coevally demonstrate cooling and enhanced productivity
- Invigoration of a wind-driven Antarctic counter current had profound effects and aided preconditioning Antarctica for glacial expansion

Supporting Information:

- Supporting Information S1
- Data Set S1

Correspondence to:

A. J. P. Houben,
alexander.houben@tno.nl

Citation:

Houben, A. J. P., Bijl, P. K., Sluijs, A., Schouten, S., & Brinkhuis, H. (2019). Late Eocene Southern Ocean cooling and invigoration of circulation preconditioned Antarctica for full-scale glaciation. *Geochemistry, Geophysics, Geosystems*, 20, 2214–2234. <https://doi.org/10.1029/2019GC008182>

Received 4 JAN 2019

Accepted 25 MAR 2019

Accepted article online 1 APR 2019

Published online 9 MAY 2019

Late Eocene Southern Ocean Cooling and Invigoration of Circulation Preconditioned Antarctica for Full-Scale Glaciation

Alexander J. P. Houben^{1,2} , Peter K. Bijl¹, Appy Sluijs¹ , Stefan Schouten³, and Henk Brinkhuis^{1,3}

¹Marine Palynology and Paleoceanography, Laboratory of Palaeobotany and Palynology, Department of Earth Sciences, Faculty of Geosciences, Utrecht University, Utrecht, The Netherlands, ²Now at Geological Survey of the Netherlands (TNO), Utrecht, The Netherlands, ³Royal Netherlands Institute for sea research (NIOZ) and Utrecht University, Texel, The Netherlands

Abstract During the Eocene-Oligocene Transition (EOT; 34–33.5 Ma), Antarctic ice sheets relatively rapidly expanded, leading to the first continent-scale glaciation of the Cenozoic. Declining atmospheric CO₂ concentrations and associated feedbacks have been invoked as underlying mechanisms, but the role of the quasi-coeval opening of Southern Ocean gateways (Tasman Gateway and Drake Passage) and resulting changes in ocean circulation is as yet poorly understood. Definitive field evidence from EOT sedimentary successions from the Antarctic margin and the Southern Ocean is lacking, also because the few available sequences are often incomplete and poorly dated, hampering detailed paleoceanographic and paleoclimatic analysis. Here we use organic dinoflagellate cysts (dinocysts) to date and correlate critical Southern Ocean EOT successions. We demonstrate that widespread winnowed glauconite-rich lithological units were deposited ubiquitously and simultaneously in relatively shallow-marine environments at various Southern Ocean localities, starting in the late Eocene (~35.7 Ma). Based on organic biomarker paleothermometry and quantitative dinocyst distribution patterns, we analyze Southern Ocean paleoceanographic change across the EOT. We obtain strong indications for invigorated surface and bottom water circulation at sites affected by polar westward-flowing wind-driven currents, including a westward-flowing Antarctic Countercurrent, starting at about 35.7 Ma. The mechanism for this oceanographic invigoration remains poorly understood. The circum-Antarctic expression of the phenomenon suggests that, rather than triggered by tectonic deepening of the Tasman Gateway, progressive pre-EOT atmospheric cooling played an important role. At localities affected by the Antarctic Countercurrent, sea surface productivity increased and simultaneously circum-Antarctic surface waters cooled. We surmise that combined, these processes contributed to preconditioning the Antarctic continent for glaciation.

Plain Language Summary The ice sheets of Antarctica are geologically a relatively recent phenomenon. Only by the end of the Eocene Epoch (±34 million years ago), major ice sheets began to develop, likely related to declining greenhouse gas concentrations. We still do not understand what the role—if any—of the tectonic openings of key land bridges (i.e., the present-day ocean conduits between Antarctica and Tasmania and the southern tip of South America) was in cooling the Antarctic continent and stimulating it to become glaciated. In this study we use organic marine microfossils to date and correlate several marginal marine sediment successions, dispersed throughout the Southern Ocean. We then show that the sediment composition at these sites changed abruptly throughout the Southern Ocean by about 35.7 million years ago, roughly two million years before the ice sheets rapidly expanded. We interpret this change in sediment composition to reflect enhanced surface ocean circulation. We furthermore analyzed chemical fossils to derive changes in past sea-water temperatures. By combining these data with counts of the marine organic microfossil species, we reconstructed past environmental change across the periods prior, during and after the growth of the Antarctic ice sheets. The results indicate that from about 35.7 million years ago onward, enhanced surface ocean circulation led to sediment winnowing, higher biological productivity in- and cooling of the surface waters around Antarctica. Irrespective of deepening of the Tasman Conduit, progressive intensification of ocean currents, probably as a result of stronger atmospheric circulation need to be considered in understanding the conditions that allowed rapid Antarctic ice sheet to expansion.

1. Introduction

A central paradigm in paleoceanography links Antarctic cryosphere development during the Eocene-Oligocene Transition (EOT; 34–33.5 Ma) to opening and deepening of Southern Ocean gateways (Kennett, 1977; Kennett et al., 1974). Tectonic separation of these gateways would have allowed for the development of a wind-driven, eastward-flowing circumpolar circulation pattern akin to the modern Antarctic Circumpolar Current, deflecting warm subtropical currents and thereby reducing ocean heat transport to Antarctica. Later work revealed that pre-glacial (early Paleogene) Antarctica was not kept “abnormally warm” by such low-latitude-derived currents (Hill et al., 2013; Huber et al., 2004). Rather, declining atmospheric CO₂ concentrations were proposed to have principally driven Eocene cooling and Eocene-Oligocene climate change (Anagnostou et al., 2016; Cramwinckel et al., 2018; DeConto & Pollard, 2003; Goldner et al., 2014; Pearson et al., 2009). Nonetheless, recent work has shown that the establishment of a westward proto-Antarctic Countercurrent resulting from initial deepening of the southern Tasman Gateway accompanied Antarctic climatic cooling in the latest early Eocene, ~49–50 Ma (Bijl, Bendle, et al., 2013; Sijp et al., 2016). This implies that paleogeographic reconfigurations and Southern Ocean gateway opening (Sijp et al., 2014) may at some level have affected Antarctic climate and Eocene-Oligocene glaciation via regional atmospheric and oceanic cooling as well. Similar to the modern, relatively shallow marine currents are primarily wind-driven. Therefore, changes in ocean-atmosphere circulation may have indeed affected Antarctic continental climate, based on model experiments (DeConto et al., 2007; DeConto & Pollard, 2003; Gasson et al., 2016). As a corollary, whereas long-term reductions in atmospheric CO₂ concentrations were required to drive glaciation, invigorated circumpolar circulation may have “set the threshold,” that is, determined the timing and nature of subsequent cryosphere development (e.g., DeConto & Pollard, 2003). In effect, the onset of Antarctic glaciation across the EOT occurred in a stepwise pattern as reflected in oxygen stable isotopes derived from benthic foraminifera (Scher et al., 2011), with the Oligocene Isotope Event 1 (Oi-1, *sensu* Katz et al., 2008) now thought to mark the onset of major glaciation.

Detailed oceanographic reconstructions from multiple regions in the Southern Ocean are required to test whether and how oceanographic changes played a role in Antarctic cryosphere development. The available evidence for warm-temperate late Eocene conditions (Gulick et al., 2017; Passchier et al., 2013; Warny et al., 2018) coexists with evidence for pre-EOT glaciation and cooling (Carter et al., 2017; Scher et al., 2014). Yet the few available shallow-marine, near-shore sedimentary sequences spanning the EOT are incomplete and generally lack sufficient accurate age assessment. This is principally because carbonate-based microfossils traditionally employed for age correlation as well as temperature proxies are poorly preserved and diagenetically altered (Billups & Schrag, 2003; Bohaty et al., 2012) or absent altogether in high-latitude environments (Cooper & O'Brien, 2004; Escutia et al., 2008; Exon et al., 2001; Florindo et al., 2003).

Relationships between climate and the surface oceanographic evolution of the Southern Ocean therefore remain elusive. On the basis of a literature survey, we identify a distinct shift from organic-rich siliciclastic silty clays to likely condensed, typically glauconite-rich facies at numerous typically neritic circum-Antarctic locations (Figure 1), which are on the basis of current biostratigraphic data of late Eocene to early Oligocene age. The precise chronostratigraphic position of this lithological shift is still poorly constrained. At Ocean Drilling Program (ODP) Site 1172 on the East Tasman Plateau, combined organic walled dinoflagellate cyst- (dinocyst) and diatom-based biostratigraphy and magnetostratigraphy suggest an unequivocal late Eocene age for the onset of this glauconite-rich section (e.g., Stickley et al., 2004; Stickley et al., 2004). The shift was originally interpreted to reflect winnowing through invigorated bottom water activity in response to Tasman Gateway deepening.

Here we aim to evaluate if the other, so-called “greensand” units reported from the mostly marginal marine Southern Ocean sites may have the same age and to explore possible relationships. To this end, we revisited five upper Eocene to lower Oligocene Antarctic/Southern Ocean sedimentary sequences to update their age models using the now available chronostratigraphic calibration of regional Paleogene dinocyst events (Bijl et al., 2013; Bijl et al., 2018; Houben et al., 2011). This also fills a gap in dinocyst biostratigraphic zonations for the Southern Ocean (Bijl et al., 2018; Bijl, Sluijs, & Brinkhuis, 2013). An update of these zonations, now also covering the Eocene-Oligocene transition interval is provided in Supporting Information S1 (Brinkhuis, 1994; Brinkhuis et al., 2003; Eldrett et al., 2004; Pross et al., 2010; Williams et al., 2004). In addition, we reconstruct sea surface conditions based on organic molecular compounds and quantitative dinocyst



Figure 1. Present-day location map of the Southern Hemisphere and position of investigated localities: Deep Sea Drilling Project Site 511 and Ocean Drilling Program Site (ODP) 696 in the southwest Atlantic Ocean and ODP 1128, 1168, and 1172 on the south margin of Australia. The approximate position of the sections of the Rio Turbio Fomation, Argentina, studied by Estebenet et al. (2014) are also indicated.

assemblages. We employ two organic molecular paleothermometers; the Tetraether index of 86 carbon atoms (TEX₈₆; Schouten et al., 2002) and the alkenone unsaturation index (U^k₃₇; Brassell et al., 1986; Prahl & Wakeham, 1987) on sediment sections from the East Tasman Plateau (ODP Site 1172) and the subantarctic southwest Atlantic Ocean (Deep Sea Drilling Program [DSDP] Site 511; Figure 1). For these sites and ODP Site 696 (northwestern Weddell Sea) and the Browns Creek Section (South Australian coast), we present organic-walled dinocyst assemblage data in order to reconstruct supraregional oceanographic reorganizations in the Southern Ocean surface waters.

2. Material and Methods

2.1. Material

2.1.1. ODP Site 1172

The EOT interval was recovered at ODP Site 1172 on the East Tasman Plateau in Holes 1172A and 1172D (Exon et al., 2001). Age control relies on biostratigraphy, notably dinocysts and diatoms (Bijl, Sluijs, & Brinkhuis, 2013; Sluijs et al., 2003; Stickley, Brinkhuis, McGonigal, et al., 2004) and magnetostratigraphy (Fuller & Touchard, 2004). Interpretation of the latter was complicated due to the strong normal overprint of the data. Fuller and Touchard (2004) therefore used the z intensity to interpret polarities. Despite these shortcomings, the interpretation is supported by the identification of chemostratigraphic and biostratigraphic signatures of widely documented paleoclimatic events such as the Middle

Eocene Climatic Optimum (Bijl et al., 2010) and the Paleocene Eocene Thermal Maximum (Sluijs et al., 2011, Bijl, Sluijs, & Brinkhuis, 2013). The sedimentary succession across the EOT comprises three lithostratigraphic units (Stickley, Brinkhuis, Schellenberg, et al., 2004, see Figure 2): (1) organic-rich silty mudstones of middle-early late Eocene age (unit III; up to 361.12 m below sea floor [mbsf]); (2) a stratigraphically condensed upper Eocene-lowermost Oligocene transitional unit characterized by increasing glauconite content, winnowing and hiatuses (unit II; 355.8–361.12 mbsf); and (3) an increasingly carbonate-rich Oligocene succession (unit I). The units are broadly taken to represent (1) a shallow-marine, prodeltaic setting, (2) a deeper-marine, current-swept setting, and (3) a pelagic setting (Stickley, Brinkhuis, Schellenberg, et al., 2004). Whereas previous studies focused on Hole 1172A, which was continuously cored across Neogene to middle Eocene strata (Exon et al., 2001), we herein also present results from the parallel Hole 1172D (Cores 2R–3R, 372.5–353 mbsf).

2.1.2. Browns Creek Section, Otway Basin, Victoria, Australia

The Browns Creek section (38°42′17.2″S 143°44′00.2″E) in Victoria, Australia, west of Cape Otway is exposed in two parallel gullies. It constitutes the following (informal) lithological units (following McGowran, 2009, Figure 2): (1) Johanna River sand from the unexposed base to 2-m height; (2) the Browns Creek formation (2–12 m), constituting the *Turritella* clays (2–9.5 m) and the *Notostrea* greensand (9.5–12 m); (3) the banded bryozoal marls (12–33 m); and (4) the upper *Turritella* clay unit (33–36 m), which is erosionally truncated at the top. The siliciclastic fraction of the Browns Creek Formation fines upward into the so-called *Turritella* clays. The glauconitic *Notostrea* greensand was interpreted to mark a transgression, culminating in the banded bryozoal marls (McGowran, 2009). The upper boundary of the *Turritella* clay marks an erosional surface and is overlain by sandy strata. Palynological assemblages from Browns Creek are very rich and well preserved, making it a classical section (Cookson & Eisenack, 1965).

2.1.3. ODP Site 1128, Australian Bight

ODP Site 1128 is located on the continental rise of Southern Australia (Feary et al., 2000, Figure 1, 134°S/127°E). We studied the interval between 397.01 and 94.16 m composite depth (mcd; Holes C and D; Figure 2). The section below 289 mcd of unit IV consists of heavily bioturbated clayey siltstone and sandy siltstone. Unit III (281.85–289 mcd) is composed of glauconitic sandstones, overlain by cross-laminated sandstones grading upward to carbonate nannofossil wackestones. Subsequently, an upper glauconitic sandstone grades upward to nannofossil carbonate mudstone. Shipboard, these sandstones were

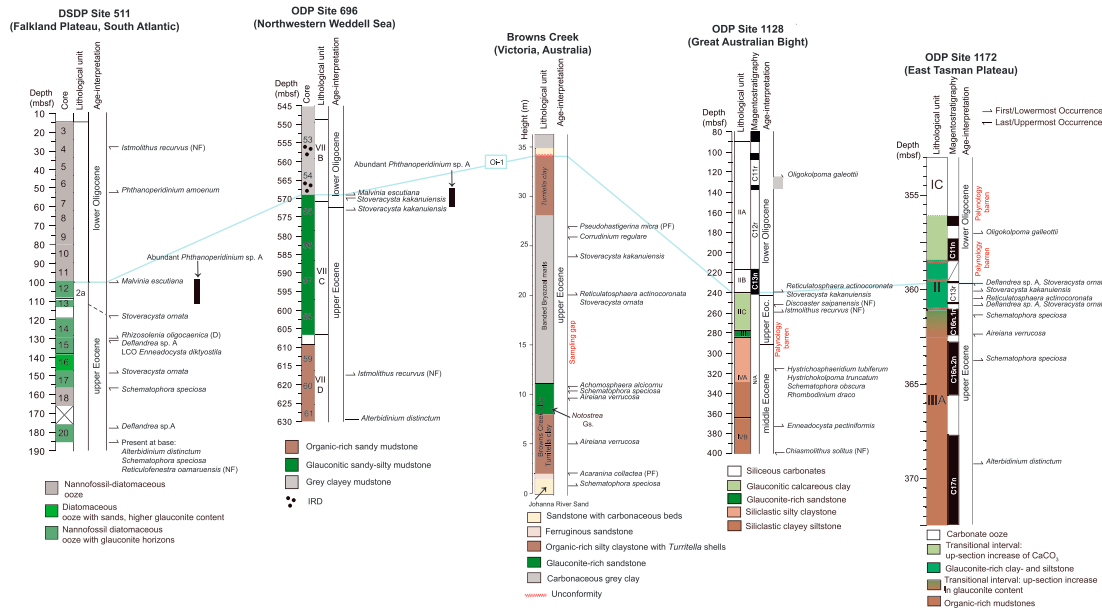


Figure 2. Biostratigraphic correlation between investigated sites. Schematic lithological columns and respective legends are indicated below the respective vertical sections. This section needed to be removed after modifications made to the figure during revision. Apologies for that. The blue horizontal line represents the correlative level of the Oligocene Isotope Event 1 (Oi-1) shift, the main phase of Antarctic cryosphere expansion. DSDP = Deep Sea Drilling Program; ODP = Ocean Drilling Program; mbsf = meters below sea floor; NF = nannofossil foraminifer bioevent; PF = planktonic foraminifer bioevent.

interpreted as turbidites separated by green burrowed claystones (Feary et al., 2000). The overlying succession of unit II is uniform green, slightly calcareous claystone that is locally interrupted, particularly in the upper parts, by a few beds of redeposited planktonic foraminiferal and nannofossil ooze and glauconite grains (Feary et al., 2000).

2.1.4. ODP Site 696, Northwestern Weddell Sea

ODP Site 696 was drilled on the South Orkney microcontinent in the northwestern Weddell Sea (Barker & Kennett, 1988; 61°S; 42°W). Unit VII (up to 548 mbsf) was divided in four subunits (Figure 2): Subunit VIID (645.6–606.9 mbsf) represents organic-rich sandy mudstone with occasional clayey mudstones throughout. Subunit VIID contains abundant macrofossil shells and shell fragments. Subunit VIIC (569.7–606.9 mbsf) yields high amounts of glauconite. The upper part of this subunit (569.7 to 579.4 mbsf) is dominantly sandy and silty mudstones. The major lithologies within subunit VIIB (548.9–579.4 mbsf) are dark claystone and clayey mudstone. At the base of this subunit, silty mudstone occurs; both lithologies contain some glauconite. Small (0.3–2 cm) rounded sedimentary features interpreted as iceberg rafted debris occur in Cores 53R and 54R (Carter et al., 2017). These ice rafted debris clasts were interpreted as derived from the Weddell Sea hinterland and Dronning Maud land, Antarctica, and to be brought to the South Orkney microcontinent via large icebergs (Carter et al., 2017), in spite of indications of warm-temperate conditions in the middle-late Eocene Southern Ocean (e.g., Bijl et al., 2009, 2010; Douglas et al., 2014).

2.1.5. DSDP Site 511, Southwest Atlantic (Falkland Plateau)

The recovered sedimentary succession at DSDP Site 511 from the western part of the Falkland Plateau, South Atlantic (Ludwig et al., 1980, 51°S, 46°W, Figure 1), yields a 163-m-long upper Eocene to lower Oligocene succession. It comprises massive gray diatomaceous oozes and muddy nannofossil-diatomaceous oozes with variable carbonate content. The lower part (~187–100 mbsf) contains episodic sand-sized glauconite (Ludwig et al., 1980). In particular, the sediments from Core 16R are completely devoid of carbonate and characterized by high glauconite content (Figure 2).

2.2. Methods

2.2.1. Palynology

For palynology, freeze-dried samples were processed with 30% HCl and 38% HF. Residues were sieved over a 15- μ m mesh and analyzed using light microscopy to a minimum of 200 dinocysts, where

possible. Counts of <50 specimens were discarded for qualitative assessment. Dinocyst nomenclature and taxonomy, unless stated otherwise, follows that cited in Williams et al. (2017), with the exception of the taxonomic deviation of the subfamily Wetzelielloideae for which we follow Bijl et al. (2016). All materials are stored in the collection of the Laboratory of Palaeobotany and Palynology, Utrecht University.

2.2.2. Biomarker-Derived Sea Surface Temperature Records

For organic biomarker analysis, powdered and freeze-dried sediments were extracted with dichloromethane (DCM)/methanol (9:1) by using accelerated solvent extraction (Dionex). Solvents were subsequently removed by rotary evaporation under vacuum. Extracts were separated by Al₂O₃ column chromatography using hexane/DCM (9:1, v/v) and DCM/methanol (1:1, v/v) as eluents to yield apolar and polar fractions, respectively. The polar fraction was dissolved in a 99:1 hexane/propanol mixture and filtered before being analyzed for TEX₈₆ and branched isoprenoid tetraether (BIT) using high-performance liquid chromatography/atmospheric pressure chemical ionization-mass spectrometry, according to Schouten et al. (2007). The polar fraction was separated through Al₂O₃ column chromatography using hexane:DCM (1:1, v/v) to yield a “ketone” fraction. The latter was analyzed for alkenones by gas chromatography using an Agilent 6890 equipped with an on column injector. The U^k₃₇ index is converted to sea surface temperature (SST) using the calibration of Müller et al. (1998), which has a standard error of ~1.5 °C.

The relationship between thaumarchaeotal membrane lipid distribution (glycerol dialkyl glycerol tetraethers [GDGTs]) and SST was assessed by construction of an extensive global core top sediment data set (Kim et al., 2010) and appeared to be different for polar and (sub)tropical settings. Therefore, Kim et al. (2010) proposed two different calibration models: (1) a logarithmic index (TEX₈₆^L) that excludes one compound, that is, the regio-isomer of thaumarchaeol and uses a global calibration data set. (2) The logarithm of TEX₈₆ (TEX₈₆^H) includes the isomer of crenarchaeol and has the polar core top data removed from the calibration data set. Application of the two calibration models for several “deep-time” case studies, culture experiments and surface sediments led Kim et al. (2010) to suggest that the TEX₈₆^L model should be employed for temperatures below 15 °C and the TEX₈₆^H model for temperatures exceeding 15 °C. However, later applications of TEX₈₆^L revealed several shortcomings in reproducing trends seen in accompanying proxy data. In light of this, TEX₈₆^L has been abandoned for this study. We present our data using the TEX₈₆^H calibration in the main figures, with the notion that this calibration may have an unknown amount of (in high latitudes probably seasonal) bias toward warmer temperatures (see, e.g., Cramwinckel et al., 2018, and Hartman et al., 2018, for further discussion). The standard error for the TEX₈₆^H model is ±2.5 °C. Samples with a BIT index of >0.4 were discarded, since this may point toward elevated input of soil-derived GDGTs thereby affecting TEX₈₆ paleothermometry (Weijers et al., 2006). Furthermore, we test our TEX₈₆ results for overprinting influences that may cause deviation from a relationship of TEX₈₆ to sea surface temperature: the Methane Index (Zhang et al., 2011) and GDGT2/crenarchaeol ratio (Weijers et al., 2011), both signaling overprint of methanotrophic archaea contributing to the sedimentary GDGT pool, the GDGT0/crenarchaeol ratio signaling the overprint of methanogenic bacteria into the GDGT pool (Blaga et al., 2009) and influences of water depth changes that could potentially influence the sedimentary GDGT pool (Taylor et al., 2013) using the GDGT2/GDGT3 ratio.

3. Results

3.1. Dating and Correlating Southern Ocean Sites

3.1.1. Browns Creek Section, Otway Coast, Southeastern Australia

Shafik and Idnurm (1997) attempted to tie the basal 10 m of the Browns Creek Section to the Geomagnetic Polarity Time Scale by generating a magnetic reversal stratigraphy. They identified two reversed polarity zones and suggested the interval to correlate to Chrons C16n.2n through C15n (~36.7–35 Ma) primarily based on relatively sparse calcareous nannofossil assemblages. The last occurrence (LO) of the typical middle Eocene foraminifer *Acaranina collectea* (Agnini et al., 2011) is located below the Browns Creek Clay (McGowran, 2009). This suggests correlation to the earliest-late-Eocene Chron C17n.2n for the base of the section. Dinocysts indicate that the Browns Creek Clay and *Notostrea* greensand are somewhat older than proposed by Shafik and Idnurm (1997). The first occurrence (FO) of *Aireiana verrucosa* at 5 m

(Figure 2) is calibrated to Chron C16n.2n and has a FO in the lower part of the Browns Creek Clay. The LO of *A. verrucosa* is calibrated against C16n.1n and is recorded just below the base of the Greensand. Hence, most of the Browns Creek *Turritella* clay corresponds to Chron C16n.2n. In the upper part of the Greensand Unit, we record the LOs of *Schematophora speciosa* and *Hemiplaciphora semilunifera* (Figure 2). These clearly predate C15n at ODP Site 1172 and at ODP Site 1168 (Sluijs et al., 2003). Furthermore, *Achomospaera alcicornu* goes extinct just below the top of the greensand unit. At ODP Site 1172, this taxon goes extinct just above the LO of *S. speciosa* and *H. semilunifera* and below the FO of *S. ornata*. On this basis, the *Notostrea* greensand corresponds to Chron C16n.1n (35.9–35.7 Ma). Above the greensand unit, there is a ~10-m sampling gap for palynology because of inaccessibility of the outcrop. Nevertheless, as expected, the marker species *Reticulatosphaera actinocoronata* and *Stoveracysta ornata* have a coeval FO at the lowermost sample within the overlying banded bryozoal marls (22-m height). Endemic Transantarctic taxa such as *Deflandrea* sp. A and *Turbiosphaera sagena* are not recorded. The FO of *Stoveracysta kakanuiensis* at 28.9-m height indicates that the upper part of the bryozoal marls approximates the initiation of the EOT (e.g., Chron C13r, ~34.7 Ma). The LOs of the foraminifers *Pseudohastigerina micra* and *Tenuitella insolita* are recorded close to the FO of *S. kakanuiensis* (McGowran, 2009). Especially *P. micra* is well constrained to just predate the Eocene-Oligocene boundary (Wade et al., 2011). *S. kakanuiensis* ranges to the top of the section. This suggests the section does not range into the Oligocene, despite the apparent unconformity above the upper *Turritella* clay unit.

3.1.2. ODP Site 1128, Great Australian Bight

We record the characteristic lower-middle Eocene dinocyst taxa *Wilsonidium echinosuturatum*, *Schematophora obscura*, *Rhombodinium draco*, and *Hystriocholpoma truncatum* in the interval between 375 and 317 mcd (Figure 2). Below that interval, two palynologically productive samples were recovered at 397 and 376 mcd. These yield taxa that are characteristic for the lower/middle Eocene boundary, notably *Cleistosphaeridium diversispinosum* and *Homotryblium tasmaniense*. Assemblages assignable to nannofossil zone NP16 of middle Eocene age occur between 350.5 and 300.1 mcd (Feary et al., 2000). In the palynologically barren interval, calcareous nannofossil assemblages at 284.03 and 289.01 mcd indicate an early late Eocene age (Zone NP18). At 254.66 mbsf, nannofossil assemblages correspond to the late Eocene (~35 Ma, upper part of Zone NP19–NP20). This implies that the onset of glauconite-rich deposition (Unit III and IIC) occurred in the late Eocene, synchronous to ODP Site 1172 and Browns Creek.

Early Oligocene calcareous nannofossil assemblages (Zone NP21–NP22) occur from 240.35 mcd (1128C-26X-CC) through 84.82 mcd (1128C-9H CC). Combined paleomagnetic and stable isotope records identify the Oi-1 shift at the base (242 mcd) of Chron C13n (242–214 mcd; Garza & Fuller, 2002; Mallinson et al., 2003). At and above 237 mcd, rich dinocyst assemblages are again recovered. The latest Eocene-early Oligocene taxa *Reticulatosphaera actinocoronata*, *Stoveracysta kakanuiensis*, and the previously undescribed taxon we recorded at Browns Creek (dinocyst sp. 2) is recorded at 237 mbsf, which is the first productive sample stratigraphically above the barren interval at 317.7 mbsf. The presence of these taxa thus suggests correlation to Chron C13n. Glauconite-rich deposition thus ended more or less coevally with the Oi-1 shift. Further up-section (120–130 mbsf), samples are again barren of palynomorphs. One productive sample was recovered from 116.47 mbsf. This level approximately correlates to the early Oligocene magnetochron C12r (Garza & Fuller, 2002). In this sample we record a typical mid-low latitude assemblage constituting *Operculodinium tiara* and *Oligokolpoma galeottii*, similar to observations from ODP Site 1172.

3.1.3. ODP Site 696, Weddell Sea

For the lower part of the succession, stratigraphic control is obtained from calcareous nannofossils, in particular the first common occurrence of *Istmolithus recurvus* (Core 59R-CC, 130 mbsf; Wei & Wise, 1990). This places the base of the investigated interval at the correlative level of the base of C16r (36.9 Ma; Villa et al., 2008). Further up-section, dinocysts are instrumental in providing age control; the FO of *Stoveracysta kakanuiensis* (571.98–571.15 mbsf) is calibrated to the latest Eocene Chron C13r at the ODP Site 1172 (34 Ma). The FO of *S. kakanuiensis* precedes the FO of the Oi-1 marker *M. escutiana* (567.39–568.83 mbsf), which suggests that the EOT is recovered. The interval between the FO of *S. kakanuiensis* and the FO of *M. escutiana* is characterized by abundant occurrences of *Phthanoperidinium* sp. A sensu Goodman and Ford 1983. This taxon is also abundant in coeval strata at DSDP Site 511, supporting the ensuing correlation. The

assemblage is, however, substantially less diverse compared to the other sites investigated. The combined palynofossil and nannofossil data provide as a reasonable base for interpreting the upper Eocene glauconite-rich unit to predate the Oi-1 level at ODP Site 696.

3.1.4. Deep Sea Drilling Project Site 511, Falkland Plateau

At DSDP Site 511, relatively rich assemblages of calcareous nannofossils (Wise, 1983) and diatoms (Gombos & Ciesielski, 1983) provide biostratigraphic age control in addition to our dinocyst-based results. At the base of the succession, we record *Schematophora speciosa* and *Alterbidinium distinctum* providing a maximum age of ~36.70 Ma (Chron C16n.2n). The calcareous nannofossil *Reticulofenestra oamaruensis* is commonly recorded at these levels. According to Villa et al. (2008), this taxon first occurs in southern high latitudes at a level corresponding to Chron C16n.1n (35.9–35.7 Ma). Consequently, the combined dinocyst and calcareous nannofossil distribution provides an age of about 36 Ma for the base of investigated section. Up-section, we record the FO of *Deflandrea* sp. A sensu Brinkhuis et al., 2003 (between 178.25 and 177.18 mbsf) and the LO of *Schematophora speciosa* (148.7–147.7 mbsf). This suggests that the interval between the base of the section and 148.5 mbsf captures the upper part of Chron C16n (36–35.7 Ma). *Stoveracysta ornata* has its FO at the top of Core 17 (150.2–149.2 mbsf). This implies that Core 16, which yielded carbonate-poor winnowed and glauconite-rich sediment, corresponds to Chron C15r (35.7 Ma). The FO of the diatom *Rhizosolenia oligocaenica* in the overlying Core 15R calibrated against upper Chron C13r (Roberts et al., 2003). This thus suggests an age of about 34.1 Ma for the interval above Core 16. Hence, the phase of severe winnowing and condensation is thus coeval to the Tasman Region and apparently ends close to the EOT.

Remarkably, below Core 15R, *Enneadocysta dictyostila* is consistently present (up to 129 mbsf). This implies a last consistent occurrence correlative to Chron C13r, similar to ODP Site 1172. Scattered occurrences further up-section likely represent reworked specimens. An increase in $\delta^{18}\text{O}$ of thermocline dwelling foraminiferal (*Subbotina*) calcite at 101 mbsf is interpreted as the Oi-1 shift (33.9 Ma). Here the dinocyst *Malvinia escutiana* first occurs (100.26–100.15 mbsf; see also Houben et al., 2011). Concomitantly, we record the FOs of *Corrudinium incompositum* and the boreal cold-water taxon *Gelatia inflata*. The abundant occurrence of *Phthanoperidinium* sp. A sensu Goodman and Ford 1983 characterizes the interval below the Oi-1 shift. Except for the transient abundance of *Phthanoperidinium comatum* (90.75–35.63 mbsf) and *P. amoenum* (46.77–35.63 mbsf), no clear dinocyst events are recorded in the lower Oligocene succession. At the top of the investigated interval (27.39 mbsf), the LO of the calcareous nannofossil *Istmolithus recurvus* is recorded (32.5 Ma; Villa et al., 2008).

3.1.5. Chronostratigraphic Synthesis and Sedimentation Rates

All available paleomagnetic, diatom, and nannofossil data at the various sites support our dinocyst-based correlations (Figure 2, Table 1). The most useful and consistent dinocyst events for dating the glauconite-rich intervals and locating the level of the Oi-1 are the FO and LO of *Schematophora speciosa* and the subsequent FOs of *Stoveracysta ornata*, *Stoveracysta kakanuiensis*, and *Malvinia escutiana* (Figure 2). Significantly, the new correlations reveal that increased glauconite content and indications of sedimentary winnowing initiated more or less coevally in time along continental margins in the Southern Ocean. Except for ODP Site 696, which has a low diversity assemblage, and ODP Site 1128, which is barren of palynomorphs, the characteristic sedimentary signatures roughly coincide with the LO of *Schematophora speciosa* within the upper part of Chron C16n.1n, at ~35.7 Ma. Furthermore, these typical sedimentary characteristics are conspicuously recorded up to the Oi-1 level.

We have synthesized the calibrated dinocyst events into dinocyst zonations, which effectively fill the gap between the Paleocene-Eocene zonations of Bijl, Sluijs, and Brinkhuis (2013) and the Oligocene-Miocene of Bijl et al. (2018) in Supporting Information S1. In order to evaluate the apparent synchronicity of “greensand” deposition and potential effects on sedimentation rates, we provide age-depths plots using the primary biostratigraphic and chemostratigraphic constraints discussed in the sections above (see Figure 3 and Data Set S1). This illustrates that the onset of “greensand deposition” is indeed more or less coeval at all investigated sites. At ODP Site 1172, Browns Creek, and ODP Site 1128, it follows that there is an evident concomitant reduction in sedimentation rate, indeed likely related to condensation and/or discontinuities, starting between 36 and 35.5 Ma. Sedimentation rates cannot be accurately constrained at DSDP Site 511 and at ODP Site 696 yet, partly because the underlying lower upper Eocene section was not recovered or preserved at these sites.

Table 1
Stratigraphic Criteria Used for the Construction of Figure 3

Site	Depth/height (m)	Age	Criterion	Type
ODP Hole 1172A	360.5	35.71	Top C16n.1n	Paleomagnetic reversal
ODP Hole 1172A	361.3	35.59	Base C16.1n	Paleomagnetic reversal
ODP Hole 1172A	361.5	36.05	Top C16n.2n	Paleomagnetic reversal
ODP Hole 1172A	365	36.7	Base C16n.2n	Paleomagnetic reversal
ODP Hole 1172A	367.1	37.75	Top C17n.1n	Paleomagnetic reversal
ODP Hole 1172A	373.9	38.33	Base C17n.3n	Paleomagnetic reversal
ODP Hole 1172A	382.1	39.63	Top C18n.1n	Paleomagnetic reversal
ODP Hole 1172A	413.6	39.7	Top C18n.2n	Paleomagnetic reversal
ODP Hole 1172A	415	40.24	Base C18n.2n	Paleomagnetic reversal
ODP Hole 1172D	356.6	29.74	Base C11n.1n	Paleomagnetic reversal
ODP Hole 1172D	357.75	29.853	Top C11n.2n	Paleomagnetic reversal
ODP Hole 1172D	358.5	30.217	Base C11n.2n	Paleomagnetic reversal
ODP Hole 1172D	359.5	33.266	Top C13n	Paleomagnetic reversal
ODP Hole 1172D	359.6	33.738	Base C13n	Paleomagnetic reversal
ODP Hole 1172D	360.6	34.99	Top C15n	Paleomagnetic reversal
ODP Hole 1172D	360.75	35.29	Base C15n	Paleomagnetic reversal
ODP Hole 1172D	360.5	35.706	Top C16n.1n	Paleomagnetic reversal
ODP Hole 1172D	361	35.706	Base C15r	Paleomagnetic reversal
ODP Hole 1172D	361.3	35.89	Base C16.1n	Paleomagnetic reversal
ODP Hole 1172D	361.5	36.05	Top C16n.2n	Paleomagnetic reversal
ODP Hole 1172D	365	36.7	Base C16n.2n	Paleomagnetic reversal
ODP Hole 1172D	367.1	36.969	Top C17n.1n	Paleomagnetic reversal
ODP Hole 1172D	373.9	38.38	Base C17n.3n	Paleomagnetic reversal
ODP Hole 1172D	382.1	38.668	Top C18n.1n	Paleomagnetic reversal
ODP Hole 1172D	413.6	39.75	Top C18n.2n	Paleomagnetic reversal
ODP Hole 1172D	415	40.2	Base C18n.2n	Paleomagnetic reversal
ODP Hole 1128C	108.2	29.97	Base C11n	Paleomagnetic reversal
ODP Hole 1128C	133.7	30.59	Top C12n	Paleomagnetic reversal
ODP Hole 1128C	137.5	31.03	Base C12n	Paleomagnetic reversal
ODP Hole 1128C	142.37	32.00	LO <i>Reticulofenestra umbilicus</i>	Nannofossil event
ODP Hole 1128C	213.5	33.16	Top C13n	Paleomagnetic reversal
ODP Hole 1128C	242	33.71	Base C13n	Paleomagnetic reversal
ODP Hole 1128C	251.04	34.40	LO <i>Discoaster saipanensis</i>	Nannofossil event
ODP Hole 1128D	259.11	36.50	FO <i>Istmolithus recurvus</i>	Nannofossil event
ODP Hole 1128D	422.17	40.80	LO <i>Chiasmolithus solitus</i>	Nannofossil event
Browns Creek	28.6	34.7	FO <i>S. kakanuiensis</i>	Dinocyst event
Browns Creek	16.5	35.4	LO <i>Achomospaera alcicornu</i>	Dinocyst event
Browns Creek	16.5	35	FO <i>R. actinocoronata</i>	Dinocyst event
Browns Creek	10.35	35.75	LO <i>Schematophora speciosa</i>	Dinocyst event
Browns Creek	10.1	35.8	LO <i>Aireiana verrucosa</i>	Dinocyst event
Browns Creek	4.73	36.5	FO <i>Aireiana verrucosa</i>	Dinocyst event
Browns Creek	2	38	LO <i>Acaranina collactea</i>	Planktonic foram event
DSDP Hole 511	178.77		FO <i>R. oamaruensis</i>	Nannofossil event
DSDP Hole 511	149.70		FO <i>Stoveracysta ornata</i>	Dinocyst event
DSDP Hole 511	119.50		LO <i>Stoveracysta ornata</i>	Dinocyst event
DSDP Hole 511	101.00		Oi-1/FO <i>M. escutiana</i>	Dinocyst event
DSDP Hole 511	27.39		LO <i>I. recurvus</i>	Nannofossil event
ODP Hole 696	568.11		FO <i>Malvinia escutiana</i>	Dinocyst event
ODP Hole 696	571.57		FO <i>S. kakanuiensis</i>	Dinocyst event
ODP Hole 696	617		FO <i>I. recurvus</i>	Nannofossil event

Note. FO = first occurrence; LO = last occurrence; Oi-1 = Oligocene Isotope Event 1.

3.2. Organic-Walled Dinoflagellate Cyst Assemblages; Quantitative Characteristics

3.2.1. Site 1172

At ODP Site 1172, the early late Eocene assemblages constitute dominant trans-Antarctic forms (*Deflandrea antarctica*, *Vozzhennikovia* spp., and *Enneadocysta dictyostila*; Figure 4). Above Chron C16n.1n (35.5 Ma), cosmopolitan and low-latitude forms (mainly *Spiniferites* spp.) are recorded for the first time in

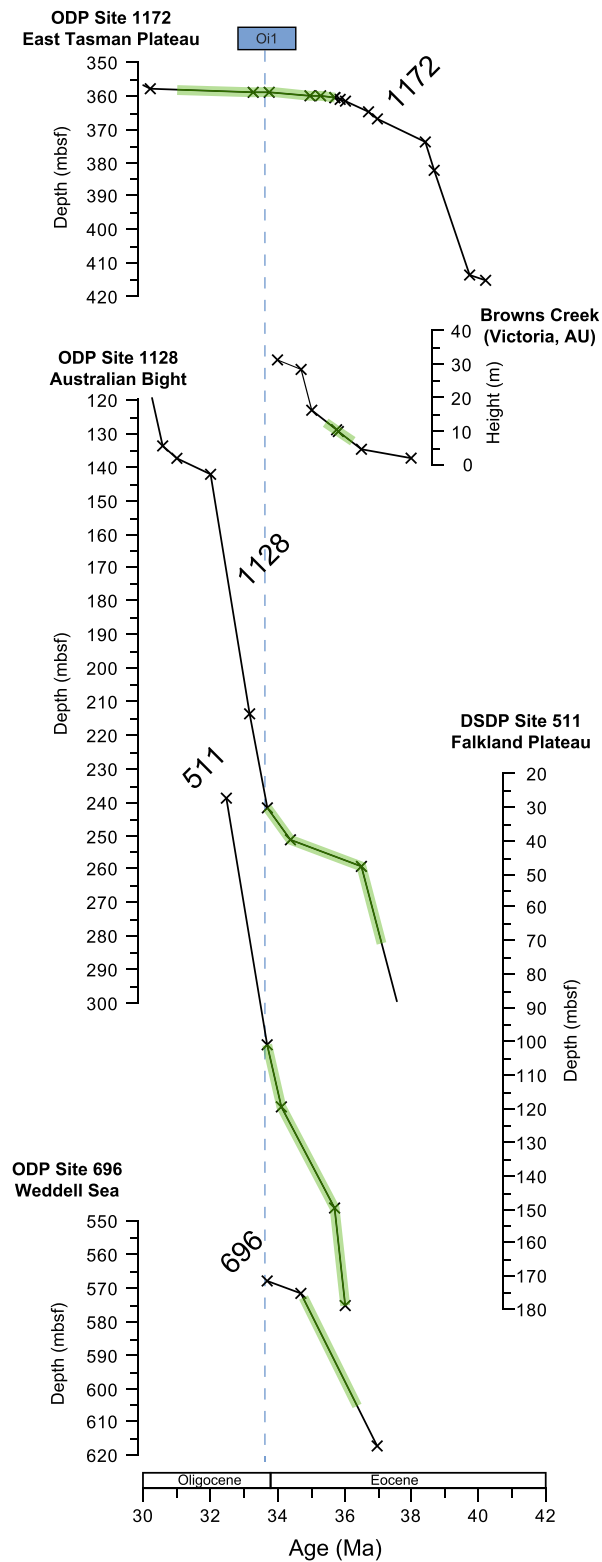


Figure 3. Age-depth relationships based on the chronostratigraphic ties discussed in this paper. An overview of the respective tie points can be found in the Table 1. The green shading illustrates the intervals characterized by glauconitic sediments. DSDP = Deep Sea Drilling Program; ODP = Ocean Drilling Program.

abundance (Figure 4). Then, progressively through the glauconite-rich unit, *Brigantedinium* spp. becomes dominant. Above a stratum which can approximately be correlated to Chron C13n and hence the EOT, the material becomes barren of palynomorphs. Above this level, palynomorphs briefly reappear in the considerably deeper pelagic facies (356.3–356.9 mbsf), and only taxa typical for low-latitude environments are recorded (e.g., *Spiniferites* spp., *Operculodinium* spp., *Hystriochokolpoma rigaudiae*, and *Oligokolpoma galeottii*).

3.2.2. Browns Creek

At the Browns Creek section, dinocyst assemblages are exceptionally rich and very well preserved (see also the pioneering work of Cookson & Eisenack, 1965). In general, distinctly different from ODP Site 1172, trans-Antarctic dinocyst taxa are not recorded. *Enneadocysta pectiniformis* occurs as the mid-low latitude counterpart species of *E. dictyostila* and specimens of *Deflandrea* primarily constitute *Deflandrea phosphoritica* (Figure 5).

Assemblages are dominated by *Spiniferites* spp., a generalist cosmopolitan taxon (Sluijs et al., 2005; Zonneveld et al., 2013, and references therein). Variations in coastal proximity throughout the record are inferred from the episodic abundance of more inshore taxa like *Dinopterygium cladoides* (in the Johanna River Sand), *Deflandrea phosphoritica*, and *Lejeunecysta fallax*. This reveals that the neritic locality was susceptible to variations in sea level and as such coastal proximity. Remarkably, throughout the *Notostrea* Greensand, the low-latitude taxa *Schematophora speciosa* and *Hemiplaciphora semilunifera* are very abundant to dominant (Figure 5). Heterotrophic representatives such as *Brigantedinium* spp. are not recorded. The upper part of the Bryozoal marls is characterized by typical outer neritic taxa (*Spiniferites* spp. and *Operculodinium* spp.). Only above the banded bryozoal marls that straddle the Eocene-Oligocene boundary, we record the abundance of heterotrophic representatives (such as *Lejeunecysta fallax*). We ascribe this to high input of riverine nutrients as the abundance of terrestrial palynomorphs is also elevated, arguably when sea level fell. Trans-Antarctic taxa remain absent throughout.

3.2.3. ODP Site 696

At the base of the investigated succession from ODP Site 696, peridinioid trans-Antarctic taxa like *Vozzhennikovia* and *Spinidinium* spp. are dominant (Figure 6), together with high abundance of *Deflandrea antarctica* and *Senegalinium* spp. and high loadings of terrestrial palynomorphs (>70%). Across the glauconite-rich upper Eocene succession of unit VIIC (607–571 mbsf), small protoperidiniaceans of the genera *Brigantedinium* and *Selenopemphix* become increasingly abundant, while the abundance of terrestrial palynomorphs declines. Just below the FO of *Stoveracysta kakanuiensis*, *Brigantedinium* spp. becomes dominant, and large specimens of other protoperidiniaceans like *Lejeunecysta* and *Selenopemphix* are recorded. Between 569.39 and 568.32 mbsf, bracketing the FO of *M. escutiana*, *Phthanoperidinium* sp. A sensu Goodman and Ford, 1983 is dominant. Throughout the lower Oligocene succession, protoperidiniacean taxa are consistently dominant, and large specimens of *Selenopemphix* and *Lejeunecysta* are present.

3.2.4. DSDP Site 511

At DSDP Site 511, dinocyst assemblages can essentially be divided in two main domains; those from below the Oi-1 shift (101 mbsf, Figure 7) and

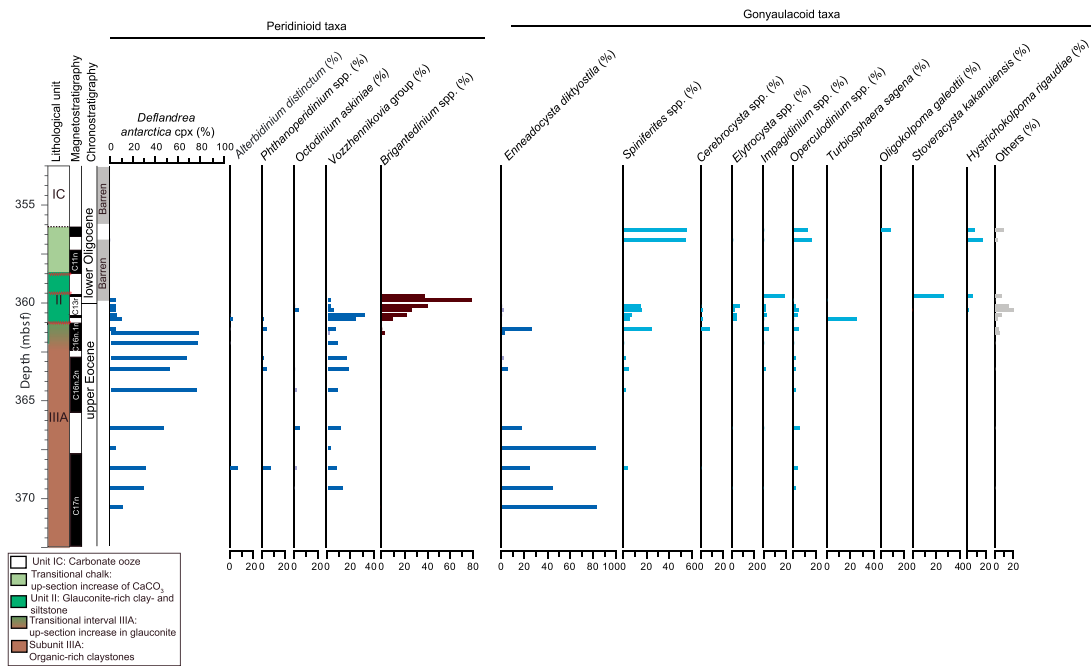


Figure 4. Relative abundance of selected dinoflagellate cyst taxa and groups encountered at Ocean Drilling Program Site 1172. Blue indicate transantarctic taxa and blue-green those with a cosmopolitan distribution. Brown indicates protoperidiniacean taxa.

those from above. Below the Oi-1 shift, endemic trans-Antarctic predominantly peridinioid taxa such as *Alterbidinium distinctum*, *Vozzhennikovia apertura*, *Deflandrea antarctica*, and *Phthanoperidinium* spp. are dominant (Figure 7). The latter group also includes high latitude taxa encountered in the northern Hemisphere (Firth, 1996; Sangiorgi et al., 2008). *Brigantedinium* spp. becomes progressively dominant in Cores 16R and Core 15R (127–142 mbsf), in association with high glauconite content. Just below the Oi-1 level, *Phthanoperidinium* sp. A sensu Goodman and Ford 1983 is dominant (Figure 7). Although the protoperidiniacean taxon *Malvinia escutiana* exhibits its FO within the body of the Oi-1 shift (see also Houben et al., 2011), other presumed heterotrophic representatives (peridinioid and protoperidiniacean taxa, see also Sluijs et al., 2005) demise in abundance and are replaced by typically offshore gonyaulacoid taxa like *Tectatodinium* spp., *Paucisphaeridium* spp., *Elytrocysta* spp., *Cerebrocysta* spp., *Impagidinium*

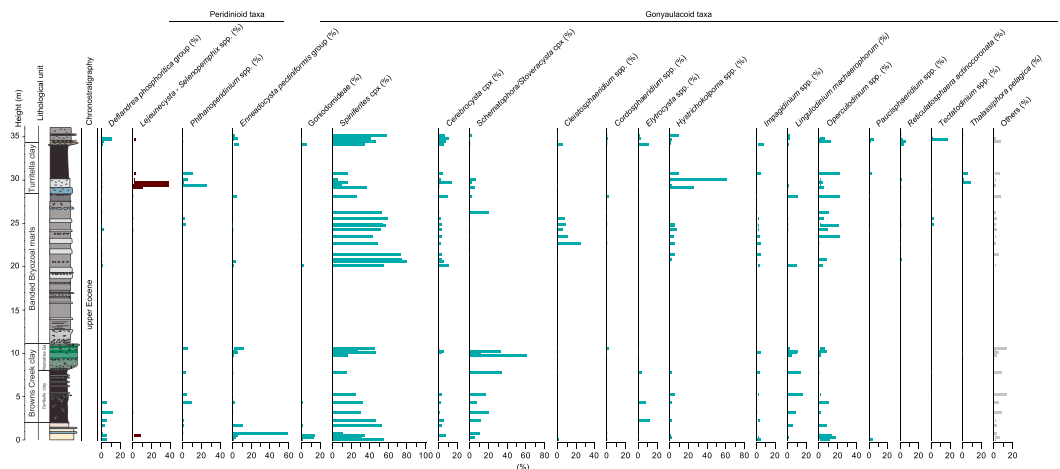


Figure 5. Relative abundance of selected dinoflagellate cyst taxa and groups encountered at Browns Creek. Blue indicate transantarctic taxa and blue-green those with a cosmopolitan distribution. Brown indicates protoperidiniacean taxa.

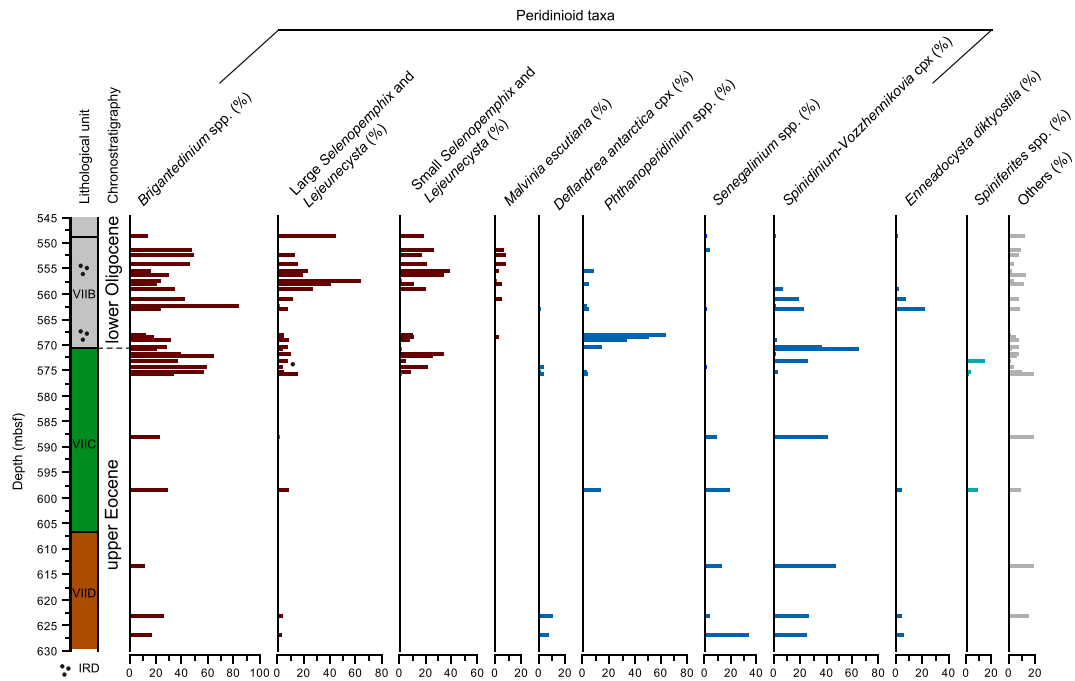


Figure 6. Relative abundance of selected dinoflagellate cyst taxa and groups encountered at Ocean Drilling Program Site 696. Blue indicate transantarctic taxa and blue-green those with a cosmopolitan distribution. Brown indicates protoperidiniacean taxa.

spp., and *Operculodinium* spp. Typical Eocene taxa assigned to the trans-Antarctic flora only extend in low abundance across the Oi-1 shift. Possibly, these are reworked.

3.3. Sea Surface Temperature Reconstructions

3.3.1. ODP Site 1172

For the samples which had BIT values below 0.4 and thus which were retained in our SST reconstruction at Site 1172, none of the indices signal overprints of methanogenesis, methanotrophic bacteria, or water depth (see Table 1). This lends confidence to present our TEX_{86} results in terms of SST. Some of the samples that

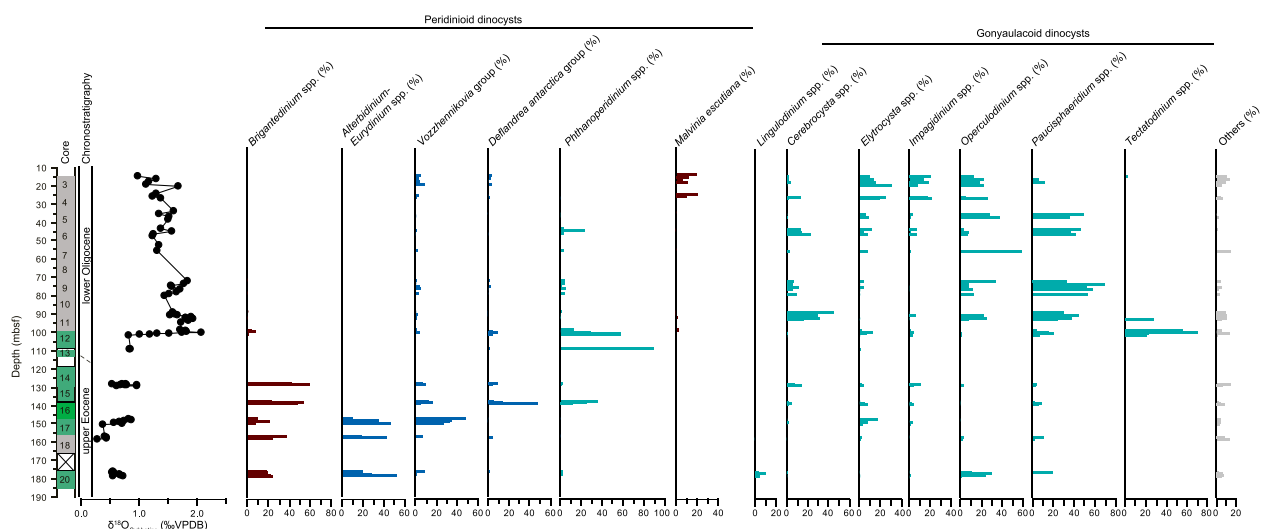


Figure 7. Relative abundance of selected dinoflagellate cyst taxa and groups encountered at Ocean Drilling Program Site 511. Blue indicate transantarctic taxa and blue-green those with a cosmopolitan distribution. Brown indicates protoperidiniacean taxa.

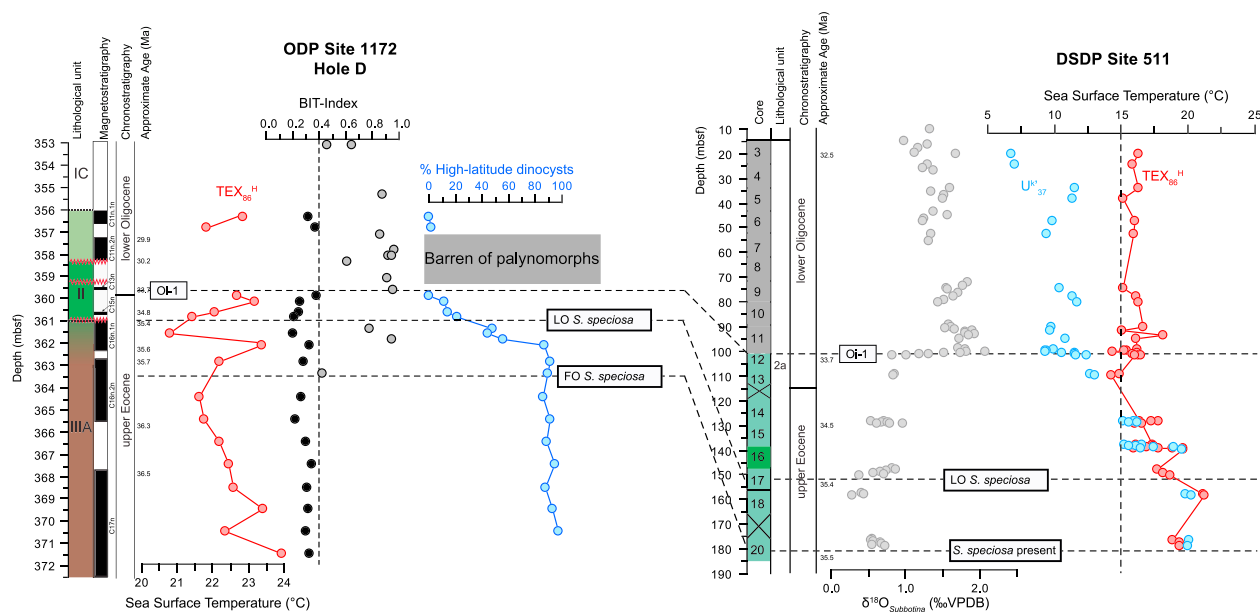


Figure 8. Sea surface temperature records from ODP Hole 1172 (left) and DSDP Site 511 (right). For DSDP Site 511, the oxygen isotope data (after Liu et al., 2009) are also indicated to illustrate the position of the Oligocene Isotope Event 1 (Oi-1) shift. Green shading indicates sedimentary successions characterized by elevated glauconite content. Glauconite content gradually increases initially near the top of unit IIIA at ODP Site 1172. At DSDP Site 511, Core 16R is particularly characterized by high glauconite content. High branched isoprenoid tetraether-index values indicate the dominance of soil-derived glycerol dialkyl glycerol tetraethers over marine glycerol dialkyl glycerol tetraethers. These samples are not considered for Tetraether index of 86 carbon atoms analysis. Dashed lines indicate correlations between both sites. Approximate ages are given at the left of the graphs. At Site 1172, the decrease of trans-Antarctic dinocyst taxa coincides with the local introduction of warmer-temperature surface waters. This is ascribed to the introduction of the proto-Leeuwin Current into the East Tasman Plateau region. DSDP = Deep Sea Drilling Program; ODP = Ocean Drilling Program.

did have high BIT index values did also have an abnormally low ring index (<1.0) or abnormally high GDGT0/crenarchaeol ratio (>10), but these samples were already discarded based on their high BIT index values. Our TEX_{86}^H analyses indicate that within the late Eocene (37–35.8 Ma; 372–364 mbsf), SSTs gradually dropped by $\sim 3^\circ\text{C}$ from 24 to 21 $^\circ\text{C}$ (Figure 8) at Site 1172. These SSTs are in-line with $U^{k'}_{37}$ -derived SSTs for the early late Eocene (Bijl et al., 2009, 2010), also when these TEX_{86}^H results are recalibrated with the TEX_{86}^H calibration (Bijl, Bendle, et al., 2013). Subsequently, SSTs (364–362 mbsf) rose by $\sim 2^\circ\text{C}$. Within the transitional sediments of uppermost units IIIA and II, TEX_{86}^H -derived SST estimates are discarded for the samples exhibiting BIT indices with values >0.4 (gray dots in Figure 8). These occur at levels that are also barren of palynomorphs. This suggests the presence of degraded marine organic material under oxygenated conditions, which leads to an enrichment in terrestrial organic matter and elevated BIT values (Huguet et al., 2009). Alkenones are not detected within the transitional sediments. Within uppermost unit IIIA (361.5 mbsf, corresponding to Chron C16n.1n, ~ 35.5 Ma), one sample denotes a distinct cooling to 21 $^\circ\text{C}$. SSTs gradually increased across transitional unit II extending into the latest Eocene (35.4 to ~ 34 Ma) by 2 $^\circ\text{C}$. Above the correlative Oi-1 level (359.6 mbsf), the early Oligocene succession is virtually barren of organic matter up to 357 mbsf. Two early Oligocene samples (dated ~ 30 Ma) reveal SSTs slightly warmer than those recorded in the late Eocene $\sim 22^\circ\text{C}$.

3.3.2. DSDP Site 511

As for Site 1172, also the TEX_{86} results from 511 can be confidently interpreted in terms of SST, as all indices to signal potential nontemperature overprints show normal values (see Data Set S1). At the base of the studied succession at Site 511 (179–176 mbsf, ~ 35.8 Ma, >35.4 Ma), SSTs are $\sim 19^\circ\text{C}$ according to both TEX_{86}^H and $U^{k'}_{37}$. At 148.2 mbsf (~ 35 Ma, Figure 8), SSTs have dropped to 18 $^\circ\text{C}$ (TEX_{86}^H), while alkenones were not detected at this level. Across Core 16R that lacks carbonate and yields much glauconite, we record a sharp cooling to $\sim 16^\circ\text{C}$ (TEX_{86}^H) and $\sim 15^\circ\text{C}$ ($U^{k'}_{37}$). SSTs drop by $\sim 2^\circ\text{C}$ to values below 15 $^\circ\text{C}$ within Core 13 (109.6 mbsf), just below the Oi-1 shift. From this level, $U^{k'}_{37}$ reports cooler SSTs than TEX_{86}^H . At the base of the Oi-1 shift at ~ 101.8 mbsf, SSTs are 15 $^\circ\text{C}$ (TEX_{86}^H) and 13 $^\circ\text{C}$ ($U^{k'}_{37}$). Across the Oi-1 shift at

100.9 mbsf, $U^{k'}_{37}$ denotes a sustained cooling to ~ 9 °C, while TEX_{86}^H shows no change. $U^{k'}_{37}$ -derived SSTs remain colder than TEX_{86}^H above the Oi-1, with an average SST of 10.6 °C ($1\sigma = 0.9$ °C). TEX_{86}^H yield average SSTs of 16.1 °C ($1\sigma = 0.9$ °C, TEX_{86}^H).

4. Discussion

4.1. Late Eocene Invigoration of Circumantarctic Bottom Currents

The abrupt inception of increased winnowing and condensation, manifested by glauconite-rich sediments of broad late Eocene age, was first reported from the Tasman Region, particularly ODP Sites 1170–1172 (Huber et al., 2004; Stickley, Brinkhuis, Schellenberg, et al., 2004). It was here ascribed to invigorated bottom current intensity during accelerated subsidence of continental blocks such as the South Tasman Rise. Our correlations now imply that the invigoration of bottom circulation at ~ 35.7 Ma was not just restricted to the shallow-marine waters around the Tasman region. Both the near-shore localities near Cape Otway (Browns Creek) and the Great Australian Bight (ODP Site 1128), located in the Australo-Antarctic Gulf (AAG), were affected by similar processes. In addition, and conspicuously, coeval condensed greensand units are now demonstrated to occur in the northwestern Weddell Sea (ODP Site 696) and in the subantarctic southwest Atlantic (DSDP Site 511; Figure 3). In addition, Estebenet et al. (2014), also on the basis of dinocyst biostratigraphic data, suggested that a widespread occurring glauconitic interval in the upper Member of Rio Turbo Fm. of the Austral Basin of southernmost Argentina and Chile is of similar age. Taken together, these results imply that invigoration of bottom water flow was a widespread phenomenon along the margins of all Southern Ocean basins during the late Eocene, everywhere starting around 35.7 Ma.

ODP Sites 1170 and 1171 are located on South Tasman Rise, which was part of a promontory between Australia and Antarctica (Stickley, Brinkhuis, Schellenberg, et al., 2004). At these sites, the indications for bottom water current invigoration appear coincident with a late Eocene phase of accelerated deepening of the conduit (Cande & Stock, 2004; Close et al., 2009). An expected consequence of widening and deepening of a southern branch of the Tasman conduit at latitudes $>60^\circ\text{S}$ is the intensification of the wind-driven westward-flowing Antarctic Counter Current. In combination with regional deepening, this may also explain a strengthening of the bottom water flow at Site 1172 on the East Tasman Plateau, northwest of the South Tasman Rise.

Although Site U1356 from the Wilkes Land Margin does not contain an in situ record of late Eocene marine sediments, the first 30 m of the earliest Oligocene part of the record is characterized and often times dominated by reworked late Eocene dinocysts (Bijl et al., 2018; Houben et al., 2013). Notably, the lithology in this part of the record is characterized by an alternation of dark gray mudstone and green sandstones, with the dinocyst assemblages from the green sandstones being dominated by the late Eocene reworking. Although allochthonous sediments are difficult to interpret, and glauconite presence has not been confirmed, the green color of the reworked late Eocene does suggest that greensands were also deposited on the late Eocene Wilkes Land Antarctic margin and subsequently reworked into the early Oligocene strata.

In the southwest Atlantic, at Sites 696 and 511 and the onshore Austral Basin, the effects of tectonic reorganization near the Drake Passage are expected to be potentially important. Although tectonic reconstructions for Drake Passage deepening remain ambivalent, there are no clear indications for a major reorganization in the late Eocene (e.g., Hill et al., 2013; Huck et al., 2017; Lagabrielle et al., 2009; Wright et al., 2018). We therefore ascribe enhanced bottom water flow in the southwest Atlantic to enhanced circulation of its western boundary as a likely westward propagation of the Antarctic Countercurrent.

The sedimentary patterns recognized in the AAG (at the Browns Creek Section and at Site 1128) may indirectly also relate to subsidence of the Tasman region. This facilitated throughflow of the eastward proto-Leeuwin current into the Southwest Pacific through a northern Tasman conduit. This mechanism was proposed to explain the incursion of cosmopolitan components of the dinocyst and diatom assemblages at Site 1172, east of Tasmania, concomitantly with the inception of winnowed, glauconite-rich sediments (Stickley, Brinkhuis, Schellenberg, et al., 2004). Analogous to the strengthened Antarctic Counter Current, this could have invigorated bottom current intensity along the northern margin of the AAG, affecting Browns Creek and ODP Sites 1168 and 1128.

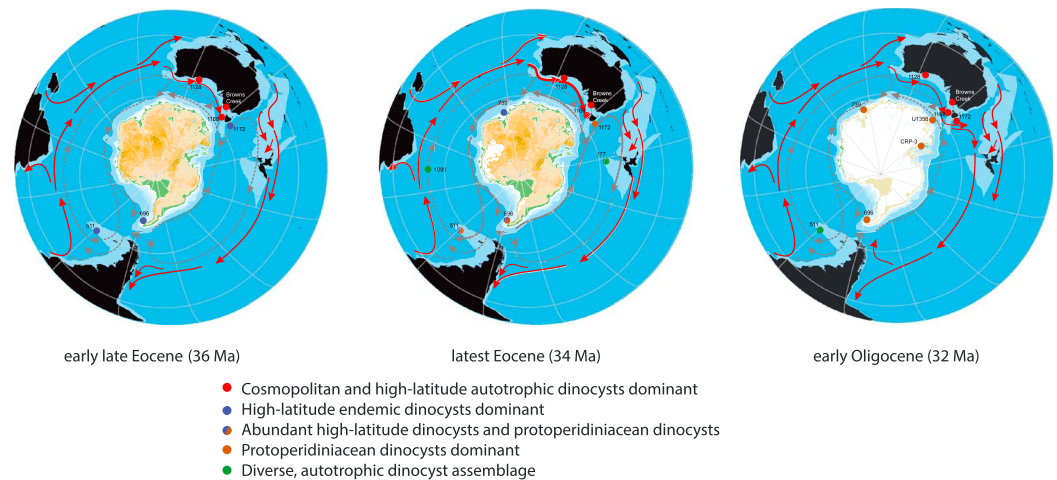


Figure 9. Synthesis of oceanographic and environmental changes between the early late Eocene, latest Eocene, and early Oligocene Southern Ocean. Colored dots indicate the generalized dinocyst assemblage composition at respective site (see legend). In the latest Eocene, SSTs have increased by 3–4 °C in the Southwest Pacific, whereas the Southwest Atlantic cooled. In the latest Eocene, westward circum-Antarctic circulation is thought to have intensified (thicker gray dashed lines). White areas on Antarctica show the presence of (ephemeral, in case of the latest Eocene) ice sheets.

4.2. Late Eocene Surface Oceanographic Change

Prior to 35.7 Ma, when glauconitic deposition started, dinocyst assemblages are dominated by low-latitude and cosmopolitan taxa in the AAG (Brown's Creek, see also ODP Site 1168 in Sluijs et al., 2003, and Bijl et al., 2011). This is likely because the surface waters were influenced by the low-latitude eastward flowing proto-Leeuwin current along the northern margin of the AAG (Figure 9), much like the Modern. Trans-Antarctic endemic dinocyst taxa are dominant at ODP Site 1172, ODP Site 696, and at DSDP Site 511, in-line with reports of similar endemic trans-Antarctic assemblages in middle-late Eocene strata from adjacent regions (e.g., Guerin et al., 2008; Mohr, 1990; Wrenn & Hart, 1988). It implies that the East Tasman Plateau, the Weddell Sea, and the southwest Atlantic were influenced by Antarctic-derived surface waters (Figure 9a). This finding confirms the sea surface circulation patterns projected by general circulation models that are primarily forced by the wind fields (e.g., Huber et al., 2004). Hence, prior to 35.7 Ma, there was a polar-easterly wind-driven surface circulation system around Antarctica, with essentially surface waters driven westward along the Antarctic margin. As part of this, the southern edge of a proto-Ross Gyre flowed along Antarctica's Pacific margin and extended northward in southwest Pacific (Tasman Current, Figure 9, see also Huber et al., 2004), and the equivalent Indian-Atlantic Southern Ocean gyre flowed westward at its southern edge and extended northward in the southwest Atlantic. This situation can be considered the equivalent of the proto- Antarctic Counter Current.

From ~35.7 Ma onward at ODP Site 1172, the abundance of cosmopolitan taxa increased (Figure 9b). In theory, these taxa could have derived from the East Australian Current, flowing southward along the eastern margin of Australia. However, the southern geographic position of Site 1172 should have kept it within the reach of the northward Tasman Current rather than the East Australian Current (e.g., Huber et al., 2004). A more likely source of the cosmopolitan dinocyst taxa is the through-flow of the eastward proto-Leeuwin Current into the southwest Pacific (Stickley, Brinkhuis, Schellenberg, et al., 2004). Yet Sites 696 and 511 remained under the influence of Antarctic-derived surface currents through the latest Eocene, also associated with phases of invigorated bottom water circulation.

Throughout the glauconite-rich unit at Site 1172 (361–359.5 mbsf; ~35.5–33.7 Ma), *Brigantedinium* spp., representative of obligate heterotrophs (*Protoperidinium*, Jacobson & Anderson, 1986; Menden-Deuer et al., 2005) that characterize high sea surface productivity, become progressively dominant (Figures 4 and 9). A similar trend is recorded at ODP Site 696 and DSDP Site 511 where *Brigantedinium* spp.

increases in abundance during the same time interval (Figure 7 and 9b). Yet, at Browns Creek in the AAG, *Schematophora speciosa* and *Hemiplaciphora semilunifera*, taxa closely related to the *Areoligera* and *Glaphyrocysta* groups, become dominant. The latter is the characteristic of relatively high-energy neritic conditions (Sluijs & Brinkhuis, 2009, and references therein), indicating the increasing *Brigantedinium* abundance does not represent a Southern Ocean wide phenomenon.

High productivity can be brought about by increased riverine or aeolian nutrient input, for which no evidence, such as increased abundance of terrestrial palynomorphs, is apparent in any of these records. Rather, we propose that high productivity is caused by increased vertical mixing of the surface waters, which also results in high abundance of *Brigantedinium* spp. in (sub)modern open oceanic environments (e.g., Marret & Zonneveld, 2003; Reichart & Brinkhuis, 2003). Further evidence for elevated surface productivity comes from increased preservation of biogenic opal and inorganic geochemical productivity proxies at ODP Site 1090 on the Agulhas Ridge (Anderson & Delaney, 2005; Diekmann et al., 2004), ODP Site 689 (Maud Rise; Schumacher & Lazarus, 2004), and originations of modern Antarctic radiolarian taxa from 35.7 Ma onward (Lazarus et al., 2008). We therefore propose that in the “counter current perimeter” invigorated bottom water circulation was strongly coupled with invigorated surface ocean circulation, leading to more vertical mixing and primary productivity. This was likely driven by enhanced polar easterly wind fields, brought about by late Eocene cooling (Scher et al., 2014); onset of Antarctic glaciation probably invigorated atmospheric pressure gradients over the Southern Ocean.

4.3. Surface-Oceanographic Change Across the EOT

Across the onset of Antarctic glaciation marked by the second step of the EOT (i.e., Oi-1), we note a series of prominent environmental changes. At ODP Site 1172, invigoration of bottom water circulation continued, with sediments becoming barren of palynomorphs at ~33.7 Ma, probably due to overexposure to oxygen. This lasted for about 3 million years (until ~30 Ma) after which the high carbonate content and gonyaulacoid-dominated cosmopolitan-low-latitude dinocyst assemblages indicate open-ocean, oligotrophic, warm-temperate conditions. Comparable low-latitude-derived assemblages are found on the northern margin of the AAG at ODP Site 1128 (Figure 9c).

At ODP Site 696, the EOT marks the onset of sustained dominance of heterotrophic protoperidiniacean dinocysts. Along with *Brigantedinium* spp. that were already abundant by late Eocene times, we now also record large-sized specimens of *Selenopemphix* and *Lejeunecysta*. These lower Oligocene assemblages are thought to be adapted to seasonal sea-ice conditions as similar assemblages are recorded at two sites along the Wilkes Land margin, Prydz Bay, and the Ross Sea (Houben et al., 2013). Whereas the Weddell Sea area featured rafting icebergs already by late Eocene times (Carter et al., 2017). It is only until after Oi-1, when evidence from dinoflagellate cysts suggest sea ice conditions commenced around Antarctica (Houben et al., 2013).

At DSDP Site 511, we also record major biotic turnover directly associated with the Oi-1. Whereas heterotrophic representatives (peridinioid taxa and *Brigantedinium* spp.) are dominant below the Oi-1 shift, gonyaulacoid taxa that are thought to relate to autotrophic dinoflagellates are dominant above Oi-1 (Figure 9). This suggests a regional reduction in nutrient availability through a decrease in vertical ocean mixing or a regional deceleration of the surface currents affecting the southwest Atlantic. Possibly, the development of sea ice conditions along the Antarctic Margin and in the Weddell Sea affected the northward extension of the Antarctic counter current, similar to the present day situation (Nicol et al., 2000).

4.4. Temperature Change Across the EOT

The middle to late Eocene is generally assumed to represent a period of gradual, long-term cooling of Southern Ocean waters that, perhaps along with the development of some Antarctic ice, led to a positive shift recorded in deep ocean benthic foraminifera oxygen isotope records (Zachos et al., 2008). Yet the few late Eocene SST records from the Southern Ocean that are available are characterized by opposing patterns. Relatively low-resolution SST records from the Southern Ocean from Liu et al. (2009) document cooling for ODP Site 1090 (Agulhas Ridge, South Atlantic Ocean) and warming for DSDP Site 277 (Campbell Plateau, Southwest Pacific) over the ~3 Myr before Oi-1. In the two stratigraphically well-resolved sections studied here, we also find this opposite pattern. A long-term ~3–4 °C middle-late Eocene cooling is recorded at ODP Site 1172 between 37 and 35.8 Ma (Figure 8). Yet, between 35.5 and 33.7 Ma (the glauconite rich

unit), SSTs warmed by 3–4 °C. However, this warming was specific for this region; the coeval introduction of cosmopolitan and low-latitude dinocysts (Figure 8) implies the influx of warm surface waters from the AAG into the Southwest Pacific through the northern conduit of the Tasman Gateway (see section 4.2). In contrast, the record from DSDP Site 511, which is under the influence of Antarctic-derived surface waters, denotes a 5–6 °C cooling throughout late Eocene succession before the Oi-1 (Figure 8). Compared to existing records (e.g., Liu et al., 2009), we interpret this as characteristic for cooling of the higher latitudes. This is in-line with vegetation reconstructions that document late Eocene climatic deterioration on Antarctica (Francis et al., 2008, and references therein). Possibly, this cooling may have contributed to suggested late Eocene ephemeral glaciation well before the Oi-1 (Hambrey et al., 1991; Katz et al., 2008; Peters et al., 2010; Scher et al., 2014).

The record from DSDP Site 511 furthermore provides information of the climate evolution across the EOT. $U^{k'}_{37}$ denotes a progressive ~7 °C cooling through the late Eocene (179–109 mbsf, 35.6–34 Ma) and a clear accelerated cooling across the Oi-1 (101 mbsf, 33.7 Ma, see Figure 8). However, the latter cooling is not apparent in TEX_{86}^H . Interestingly, $U^{k'}_{37}$ temperatures are equivalent to TEX_{86}^H temperatures before the Oi-1 but cooler than that after Oi-1. Considering the complications with the TEX_{86} paleothermometer, it may seem that the $U^{k'}_{37}$ SSTs best reflect local temperature development. However, since $U^{k'}_{37}$ records an abrupt, sustained 3–4 °C cooling across the Oi-1, the total cooling between 35.5 and 33.4 Ma equates to about 10 °C (Figure 8). This substantially exceeds the 6 °C that would account for the 1–1.5‰ increase of deep sea benthic foraminiferal $\delta^{18}O$ records across Oi-1, even without invoking a realistic increase in continental ice volume. Thus, the $U^{k'}_{37}$ drop in temperatures exceeds those expected from general southern ocean cooling. One explanation for the exaggerated cooling in alkenone temperatures might be seasonality. There are multiple reports of increased seasonality (i.e., winter cooling) across the Oi-1 (Eldrett et al., 2009; Ivany et al., 2000; Wade et al., 2012). Although the $U^{k'}_{37}$ is calibrated to mean annual temperature (Müller et al., 1998), it has shown to reflect different seasonal temperatures at different locations (e.g., Ternois et al., 1997). As modern high-latitude haptophyte communities primarily bloom in early spring (Herbert et al., 1998), it may well be that high-latitude alkenone-derived SSTs are biased toward spring. For TEX_{86} , it has been argued that it reflects summer temperatures at high latitudes, because the dominant season of fecal pelleting and export production is during the summer (e.g., Bijl et al., 2009). This implies that cooling associated with the inception of full-scale Antarctic glaciation was amplified in winter and spring and not as much in summer. This would be in agreement with the presence of winter sea ice in the Antarctic margin regions, as this would sustain cooler winter sea surface temperatures. SST records from the late Eocene from the low latitudes and the northern hemisphere are sparse. Yet those available (e.g., Cramwinckel et al., 2018; Lear et al., 2008; Liu et al., 2009) do not evidence major cooling before the EOT, arguing that late Eocene pre-EOT cooling is primarily an Antarctic phenomenon.

4.5. Late Eocene Ocean Circulation Invigoration Preconditioned Antarctica for Glaciation

The coincidence of invigorated circulation at sites theoretically affected by the Antarctic Counter Current; enhanced sea surface productivity at these localities and the apparent cooling of the circum-Antarctic surface waters strongly suggest that positive feedbacks preconditioned the Antarctic continent for glaciation from about 35.7 Ma onward. Multiple processes could have provided the primary forcing of these changes. Evidence for late Eocene cooling is provided by deep-sea oxygen isotope data (Scher et al., 2014); cooling spurred circum-Antarctic circulation, enhanced vertical mixing, increased deep and intermediate water formation (Scher & Martin, 2006), and resulted in more productive surface waters, which is consistent with our and previous observations (Stickley, Brinkhuis, Schellenberg, et al., 2004). Goldner et al. (2014) suggested that a decrease in CO_2 concentrations initiated Antarctic Ice Sheet growth, leading to increased thermal gradients and invigorated ocean circulation. There is now increasing evidence to suggest that glaciation initiated in the late Eocene, prior to Oi-1 (Carter et al., 2017; Scher et al., 2014). Our results indicate that changes in circum-Antarctic circulation preceded Oi-1 by ~2 million years.

Initial studies arising from ODP Leg 189 in the Tasman Gateway region suggested late Eocene deepening of the Tasmanian Gateway on the basis of lithological (glauconite deposition and winnowing) and micropaleontological characteristics (Stickley, Brinkhuis, Schellenberg, et al., 2004). However, the results from Leg 189 do not unequivocally reflect deepening, as absolute water depth is difficult to interpret from lithological and microfossil data. The activation of Tasmantid Guyots in the region (Vogt & Conolly, 1971) add

to the tectonic complexity and specifically makes rapid deepening of tectonic blocks in the region implausible. Drifting between Tasmania and Antarctica commenced in the middle Eocene (~49 Ma; Williams et al., 2019). Ocean crust formation already generated a deep oceanographic conduit by that time and consequently gradual deepening of the conjugate margins is expected (Totterdell et al., 2000). Indeed, the gradual increase in carbonate content at Site 1172 during the Middle Eocene can be interpreted as a gradual deepening of the East Tasman Plateau (Röhl et al., 2004), which decreases the possible extent of further rapid deepening at the time of greensand deposition. Irrespective of the validity of inferred rapid deepening at 35.7 Ma (Stickley, Brinkhuis, Schellenberg, et al., 2004), the enhanced circum-Antarctic Counter Current flow, may have contributed to thermal isolation, and cooling of the margins of the Antarctic continent thereby intensifying the polar high-pressure cell, leading to stronger polar wind fields. In our view, the observations do not provide compelling evidence for rapid deepening of the continental shelf, but the circum-Antarctic extent of greensands actually argues against this. We therefore conclude that the root cause of greensands is likely related to atmospheric-forced enhanced Southern Ocean circulation, which resulted in positive feedbacks that aided to precondition Antarctica for rapid ice growth and further circulation change at Oi-1, roughly 2 million years later.

The possibility of the onset of Antarctic Countercurrent throughflow has been tested using GCM-forced ocean model experiments (Sijp et al., 2016). These indeed reproduce westward throughflow of the Countercurrent through the Tasmanian Gateway, in accordance with field data showing the onset of Antarctic cooling and concomitant initial opening of the Tasman conduit in the earliest middle Eocene (Bijl, Bendle, et al., 2013). However, late Eocene simulations are of too coarse resolution (Hill et al., 2013) and/or feature a too northerly gateway opening to adequately represent the counter current (Sijp et al., 2011). Recent ocean model studies (Baatsen et al., 2016) for the late Eocene, under state-of-the-art geographical boundary conditions, suggest additional eastward throughflow into the southwest Pacific Ocean and may explain the greensand deposition along the south Australian margin when these currents invigorated. However, these models still cannot resolve the complex bathymetry nor did the simulations test possible topographic/bathymetric scenarios in relation to ocean flow.

Gateway tectonics may thus have caused late Eocene invigoration of Countercurrent circulation, but it may not be necessary to invoke these causally. In particular, polar amplification of CO₂-forced cooling (Cramwinckel et al., 2018; Scher et al., 2014) could have led to amplified temperature gradients and wind strength, and this could have enhanced invigoration of Southern Ocean current systems.

5. Conclusions

Our results indicate that during the late Eocene, the Antarctic Margin and south Southern Ocean were critically affected by changing and conspicuously enhanced ocean circulation. This finding points toward the inception of a potentially powerful positive climate feedback system; involving cooling, enhanced atmospheric circulation, thermal isolation, and enhanced biological productivity. This combination of processes was a determining factor in the nature and timing of ice-sheet expansion marked by the Oi-1. The late Eocene intensification of the Antarctic Countercurrent and its climatic and environmental feedbacks may have well contributed to setting the stage of minor scale, ephemeral Antarctic glaciations prior to the EOT. This pattern of transient precursor glaciations prior to the major glacial expansion is in line with the hypothesized role of powerful nonlinear feedbacks in ice sheet mass balance and stability.

References

- Agnini, C., Fornaciari, E., Giusberti, L., Grandesso, P., Lanci, L., Luciani, V., et al. (2011). Integrated biomagnetostratigraphy of the Alano section (NE Italy): A proposal for defining the middle-late Eocene boundary. *GSA Bulletin*, *123*(5–6), 841–872. <https://doi.org/10.1130/B30158.1>
- Anagnostou, E., John, E. H., Edgar, K. M., Foster, G. L., Ridgwell, A., Inglis, G. N., et al. (2016). Changing atmospheric CO₂ concentration was the primary driver of early Cenozoic climate. *Nature*, *533*, 80–384.
- Anderson, L. D., & Delaney, M. L. (2005). Middle Eocene to early Oligocene paleoceanography from Agulhas Ridge, Southern Ocean (Ocean Drilling Program Leg 177, Site 1090). *Paleoceanography*, *20*, PA3103. <https://doi.org/10.1029/2004PA001043>
- Baatsen, M., Van Hinsbergen, D. J., Heydt, A. S., Dijkstra, H. A., Sluijs, A., Abels, H. A., & Bijl, P. K. (2016). Reconstructing geographical boundary conditions for palaeoclimate modelling during the Cenozoic. *Climate of the Past*, *12*(8), 1635–1644. <https://doi.org/10.5194/cp-12-1635-2016>
- Barker, P., Kennett, J. (1988). Leg 113. Proceedings of the Ocean Drilling Program Initial Reports of Leg 113 (785 pp.).

Acknowledgments

A. H. and H. B. acknowledge Equinor for funding. A. S. thanks the European Research Council for Starting Grant 259627 and the Netherlands Earth System Science Centre. P. K. B. acknowledges funding through NWO polar programme grant 866.10.110 and Veni grant 863.13.002. We thank Steven Bohaty for numerous discussions on Southern Ocean biostratigraphy and oceanography. We thank Stephen Gallagher for guidance and assistance with sampling in Australia. The Integrated Ocean Discovery Program (IODP) provided samples and ship-board data. We acknowledge Mike Hannah, Rob McKay, and one anonymous reviewer for constructive reviews. This publication is accompanied by two supporting information files that contain a description of the dinocyst stratigraphic framework and updated zonation (Supporting Information S1) and an MS Excel file with palynological and organic paleothermometry data (Data Set S1).

- Bijl, P. K., Bendle, J. A. P., Bohaty, S. M., Pross, J., Schouten, S., Tauxe, L., et al. (2013). Eocene cooling linked to early flow across the Tasmanian Gateway. *Proceedings of the National Academy of Sciences*, *110*(24), 9645–9650. <https://doi.org/10.1073/pnas.1220872110>
- Bijl, P. K., Brinkhuis, H., Egger, L. M., Eldrett, J. S., Frieling, J., Grothe, A., et al. (2016). Comment on 'Wetzeliella and its allies—The 'hole' story: A taxonomic revision of the Paleogene dinoflagellate subfamily Wetzelielloideae' by Williams et al. (2015). *Palynology*, 423–429.
- Bijl, P. K., Houben, A. J. P., Bruls, A., Pross, J., & Sangiorgi, F. (2018). Stratigraphic calibration of Oligocene-Miocene organic-walled dinoflagellate cysts from offshore Wilkes Land, East Antarctica, and a zonation proposal. *Journal of Micropalaeontology*, *37*(1), 105–138. <https://doi.org/10.5194/jm-37-105-2018>
- Bijl, P. K., Houben, A. J. P., Schouten, S., Bohaty, S. M., Sluijs, A., Reichart, G. J., et al. (2010). Transient Middle Eocene atmospheric CO₂ and temperature variations. *Science*, *330*(6005), 819–821. <https://doi.org/10.1126/science.1193654>
- Bijl, P. K., Pross, J., Stickley, C. E., Huber, M., Guerin, R., Houben, A. J. P., et al. (2011). Environmental forcing on paleogene Southern Ocean biogeography. *Paleoceanography*, *26*, PA1202. <https://doi.org/10.1029/2009PA001905>
- Bijl, P. K., Schouten, S., Sluijs, A., Reichart, G., Zachos, J. C., & Brinkhuis, H. (2009). Early Palaeogene temperature evolution of the southwest Pacific Ocean. *Nature*, *461*(7265), 776–779. <https://doi.org/10.1038/nature08399>
- Bijl, P. K., Sluijs, A., & Brinkhuis, H. (2013). A magneto-and chemostratigraphically calibrated dinoflagellate cyst zonation of the early Palaeogene South Pacific Ocean. *Earth-Science Reviews*, *124*, 1–31. <https://doi.org/10.1016/j.earscirev.2013.04.010>
- Billups, K., & Schrag, D. P. (2003). Application of benthic foraminiferal Mg/Ca ratios to questions of Cenozoic climate change. *Earth and Planetary Science Letters*, *209*(1–2), 181–195. [https://doi.org/10.1016/S0012-821X\(03\)00067-0](https://doi.org/10.1016/S0012-821X(03)00067-0)
- Blaga, C. I., Reichart, G.-J., Heiri, O., & Sinninghe Damsté, J. S. (2009). Tetraether membrane lipid distributions in water-column particulate matter and sediments: A study of 47 European lakes along a north-south transect. *Journal of Paleolimnology*, *41*(3), 523–540. <https://doi.org/10.1007/s10933-008-9242-2>
- Bohaty, S. M., Zachos, J. C., & Delaney, M. L. (2012). Foraminiferal Mg/Ca evidence for Southern Ocean cooling across the Eocene–Oligocene transition. *Earth and Planetary Science Letters*, *317*, 251–261.
- Brassell, S. C., Eglinton, G., Marlowe, I. T., Pflaumann, U., & Sarnthein, M. (1986). Molecular stratigraphy: A new tool for climatic assessment. *Nature*, *320*(6058), 129–133. <https://doi.org/10.1038/320129a0>
- Brinkhuis, H. (1994). Late Eocene to early Oligocene dinoflagellate cysts from the Priabonian type-area (Northeast Italy): Biostratigraphy and paleoenvironmental interpretation. *Palaeogeography, Palaeoclimatology, Palaeoecology*, *107*(1–2), 121–163. [https://doi.org/10.1016/0031-0182\(94\)90168-6](https://doi.org/10.1016/0031-0182(94)90168-6)
- Brinkhuis, H., Sengers, S., Sluijs, A., Warnaar, J., & Williams, G. L. (2003). Latest cretaceous to earliest Oligocene, and quaternary dinoflagellate cysts from ODP site 1172, East Tasmanian plateau. Proceedings of the ocean drilling program. Scientific results 189.
- Cande, S. C., & Stock, J. M. (2004). Cenozoic reconstructions of the Australia–New Zealand–South Pacific sector of Antarctica. The Cenozoic Southern Ocean: Tectonics, sedimentation and climate change between Australia and Antarctica. *Geophysical Monograph Series*, *151*, 5–18.
- Carter, A., Riley, T. R., Hillenbrand, C.-D., & Rittner, M. (2017). Widespread Antarctic glaciation during the Late Eocene. *Earth and Planetary Science Letters*, *458*, 49–57. <https://doi.org/10.1016/j.epsl.2016.10.045>
- Close, D. I., Watts, A. B., & Stagg, H. M. J. (2009). A marine geophysical study of the Wilkes Land rifted continental margin, Antarctica. *Geophysical Journal International*, *177*(2), 430–450. <https://doi.org/10.1111/j.1365-246X.2008.04066.x>
- Cookson, I. C., & Eisenack, A. (1965). Microplankton from the Browns Creek Clays sw. *Proceedings of the Royal Society of Victoria*, *79*, 119–131.
- Cooper, A. K., & O'Brien, P. E. (2004). Leg 188 synthesis: Transitions in the glacial history of the Prydz Bay region, East Antarctica, from ODP drilling 188, 1–42.
- Cramwinckel, M. J., Huber, M., Kocken, I. J., Agnini, C., Bijl, P. K., Bohaty, S. M., et al. (2018). Synchronous tropical and polar temperature evolution in the Eocene. *Nature*, *559*(7714), 382–386. <https://doi.org/10.1038/s41586-018-0272-2>
- DeConto, R., Pollard, D., & Harwood, D. M. (2007). Sea ice feedback and Cenozoic evolution of Antarctic climate and ice sheets. *Paleoceanography*, *22*, PA3214. <https://doi.org/10.1029/2006PA001350>
- DeConto, R. M., & Pollard, D. (2003). Rapid Cenozoic glaciation of Antarctica induced by declining atmospheric CO₂. *Nature*, *421*(6920), 245–249. <https://doi.org/10.1038/nature01290>
- Diekmann, B., Kuhn, G., Gersonde, R., & Mackensen, A. (2004). Middle Eocene to early Miocene environmental changes in the sub-Antarctic Southern Ocean: Evidence from biogenic and terrigenous depositional patterns at ODP site 1090. *Global and Planetary Change*, *40*(3–4), 295–313. <https://doi.org/10.1016/j.gloplacha.2003.09.001>
- Douglas, P. M., Affek, H. P., Ivany, L. C., Houben, A. J., Sijp, W. P., Sluijs, A., et al. (2014). Pronounced zonal heterogeneity in Eocene southern high-latitude sea surface temperatures. *Proceedings of the National Academy of Sciences*, *111*, 6582–6587.
- Eldrett, J. S., Greenwood, D. R., Harding, I. C., & Huber, M. (2009). Increased seasonality through the Eocene to Oligocene transition in northern high latitudes. *Nature*, *459*(7249), 969–973. <https://doi.org/10.1038/nature08069>
- Eldrett, J. S., Harding, I. C., Firth, J. V., & Roberts, A. P. (2004). Magnetostratigraphic calibration of Eocene–Oligocene dinoflagellate cyst biostratigraphy from the Norwegian–Greenland Sea. *Marine Geology*, *204*(1–2), 91–127. [https://doi.org/10.1016/S0025-3227\(03\)00357-8](https://doi.org/10.1016/S0025-3227(03)00357-8)
- Escutia, C., Brinkhuis, H., & Klaus, A. (2008). Cenozoic East Antarctic ice sheet evolution from Wilkes Land margin sediments. *IODP Scientific Prospectus*, *318*. <https://doi.org/10.2204/iodp.sp.318.2008>
- Estebenet, M. S. G., Guerin, G. R., & Alperin, M. I. (2014). Dinoflagellate cyst distribution during the Middle Eocene in the Drake Passage area: Paleoclimatological implications. *Ameghiniana*, *51*(6), 500–509. <https://doi.org/10.5710/AMGH.06.08.2014.2727>
- Exon, N. J., Kennett, J. P., & Malone, M. (2001). ODP Leg 189 initial results. Proceedings of the ocean drilling program, initial reports of the ODP, College Station, TX, USA 189.
- Feary, D. A., Hine, A. C. & Malone, M. (2000). ODP Leg 182 initial results. Proceedings of the ODP, initial reports, College Station, TX, USA 182.
- Firth, J. V. (1996). Upper middle Eocene to Oligocene dinoflagellate biostratigraphy and assemblage variations in Hole 913B, Greenland Sea. In J. Thiede, A. M. Myrhe, J. V. Firth, G. L. Johnson, & W. F. Ruddiman (Eds.), *Proceedings of the Ocean Drilling Program, Scientific Results* (pp. 203–242).
- Florindo, F., Bohaty, S. M., Erwin, P. S., Richter, C., Roberts, A. P., Whalen, P. A., & Whitehead, J. M. (2003). Magnetostratigraphic chronology and palaeoenvironmental history of Cenozoic sequences from ODP sites 1165 and 1166, Prydz Bay, Antarctica. *Palaeogeography, Palaeoclimatology, Palaeoecology*, *198*(1–2), 69–100. [https://doi.org/10.1016/S0031-0182\(03\)00395-X](https://doi.org/10.1016/S0031-0182(03)00395-X)
- Francis, J. E., Marensi, S., Levy, R., Hambrey, M., Thorn, V. C., Mohr, B., et al. (2008). From greenhouse to icehouse Eocene/Oligocene in Antarctica. *Developments in Earth and Environmental Sciences*, *8*, 309–368. [https://doi.org/10.1016/S1571-9197\(08\)00008-6](https://doi.org/10.1016/S1571-9197(08)00008-6)

- Fuller, M., & Touchard, Y. (2004). On the magnetostratigraphy of the East Tasman Plateau, timing of the opening of the Tasmanian Gateway and paleoenvironmental changes. *Geophysical Monograph Series*, 151, 63–78.
- Garza, R. S. M., & Fuller, M. (2002). Paleolatitudes and magnetostratigraphy for Cenozoic sediments, ODP Leg 182: The Great Australian Bight. *Earth, Planets and Space*, 54(4), 399–413. <https://doi.org/10.1186/BF03352429>
- Gasson, E., DeConto, R. M., Pollard, D., & Levy, R. H. (2016). Dynamic Antarctic ice sheet during the early to mid-Miocene. *Proceedings of the National Academy of Sciences*, 113(13), 3459–3464. <https://doi.org/10.1073/pnas.1516130113>
- Goldner, A., Herold, N., & Huber, M. (2014). Antarctic glaciation caused ocean circulation changes at the Eocene–Oligocene transition. *Nature*, 511(7511), 574–577. <https://doi.org/10.1038/nature13597>
- Gombos, A. M., & Ciesielski, P. F. (1983). Late Eocene to Early Miocene diatoms from the southwest Atlantic. In W. J. Ludwig & V. A. Krasheninnikov (Eds.), *Initial reports of the Deep Sea Drilling Project 71* (pp. 859–977).
- Gradstein, F. M., Ogg, J. G., Schmitz, M. D., & Ogg, G. (2012). *The geologic time scale 2012* (p. 1176). Amsterdam: Elsevier.
- Guerstein, R., Guler, M. V., Williams, G. L., Fensome, R. A., & Chiesa, J. O. (2008). Middle Palaeogene dinoflagellate cysts from Tierra del Fuego, Argentina: Biostratigraphy and palaeoenvironments. *Journal of Micropaleontology*, 27(1), 75–94. <https://doi.org/10.1144/jm.27.1.75>
- Gulick, S. P. S., Shevenell, A. E., Montelli, A., Fernandez, R., Smith, C., Warny, S., et al. (2017). Initiation and long-term instability of the East Antarctic ice sheet. *Nature*, 552(7684), 225–229. <https://doi.org/10.1038/nature25026>
- Hambrey, M. J., Ehrmann, W. U., & Larsen, B. (1991). Cenozoic glacial record of the Prydz Bay continental shelf, East Antarctica. *Proceedings of the ODP - Scientific Results*, 119, 77–132.
- Hartman, J. D., Sangiorgi, F., Salabarnada, A., Peterse, F., Houben, A. J. P., Schouten, S., et al. (2018). Paleooceanography and ice sheet variability offshore Wilkes Land, Antarctica—Part 3: Insights from Oligocene–Miocene TEX₈₆-based sea surface temperature reconstructions. *Climate of the Past*, 14(9), 1275–1297. <https://doi.org/10.5194/cp-14-1275-2018>
- Herbert, T. D., Schuffert, J. D., Thomas, D., Lange, C., Weinheimer, A., & Peleo-Alampay, A. (1998). Depth and seasonality of alkenone production along the California margin inferred from a core top transect. *Paleoceanography*, 13(3), 263–271. <https://doi.org/10.1029/98PA00069>
- Hill, D. J., Haywood, A. M., Valdes, P. J., Francis, J. E., Lunt, D. J., Wade, B. S., & Bowman, V. C. (2013). Paleogeographic controls on the onset of the Antarctic circumpolar current. *Geophysical Research Letters*, 40, 5199–5204. <https://doi.org/10.1002/grl.50941>
- Houben, A. J., Bijl, P. K., Pross, J., Bohaty, S. M., Passchier, S., Stickley, C. E., et al. (2013). Reorganization of Southern Ocean plankton ecosystem at the onset of Antarctic glaciation. *Science*, 340(6130), 341–344. <https://doi.org/10.1126/science.1223646>
- Houben, A. J. P., Bijl, P. K., Guerstein, G. R., Sluijs, A., & Brinkhuis, H. (2011). *Malvinia escutiana*, a new biostratigraphically important Oligocene dinoflagellate cyst from the Southern Ocean. *Review of Palaeobotany and Palynology*, 165(3–4), 175–182. <https://doi.org/10.1016/j.revpalbo.2011.03.002>
- Huber, M., Brinkhuis, H., Stickley, C. E., Doos, K., Sluijs, A., Warnaar, J., et al. (2004). Eocene circulation of the Southern Ocean: Was Antarctica kept warm by subtropical waters? *Paleoceanography*, 19, PA4026. <https://doi.org/10.1029/2004PA001014>
- Huck, C. E., van de Flierdt, T., Bohaty, S. M., & Hammond, S. J. (2017). Antarctic climate, Southern Ocean circulation patterns, and deep water formation during the Eocene. *Paleoceanography*, 32, 674–691. <https://doi.org/10.1002/2017PA003135>
- Huguet, C., Kim, J. H., de Lange, G. J., Sinninghe Damsté, J. S. S., & Schouten, S. (2009). Effects of long term oxic degradation on the U^K₃₇, TEX₈₆ and BIT organic proxies. *Organic Geochemistry*, 40(12), 1188–1194. <https://doi.org/10.1016/j.orggeochem.2009.09.003>
- Ivany, L. C., Patterson, W. P., & Lohmann, K. C. (2000). Cooler winters as a possible cause of mass extinctions at the Eocene/Oligocene boundary. *Nature*, 407(6806), 887–890. <https://doi.org/10.1038/35038044>
- Jacobson, D. M., & Anderson, D. M. (1986). Thecate heterotrophic dinoflagellates: Feeding behavior and mechanisms. *Journal of Phycology*, 22(3), 249–258. <https://doi.org/10.1111/j.1529-8817.1986.tb00021.x>
- Katz, M. E., Miller, K. G., Wright, J. D., Wade, B. S., Browning, J. V., Cramer, B. S., & Rosenthal, Y. (2008). Stepwise transition from the Eocene greenhouse to the Oligocene icehouse. *Nature Geoscience*, 1(5), 329–334. <https://doi.org/10.1038/ngeo179>
- Kennett, J., Houtz, R., Andrews, P., Edwards, A., Gostin, V., Hajos, M., et al. (1974). Development of the circum-Antarctic current. *Science*, 186(4159), 144–147. <https://doi.org/10.1126/science.186.4159.144>
- Kennett, J. P. (1977). Cenozoic evolution of Antarctic glaciation, the circum-Antarctic Ocean, and their impact on global paleoceanography. *Journal of Geophysical Research*, 82(27), 3843–3860. <https://doi.org/10.1029/JC082i027p03843>
- Kim, J., van der Meer, J., Schouten, S., Helmke, P., Willmott, P., Sangiorgi, F., et al. (2010). New indices and calibrations derived from the distribution of crenarchaeal isoprenoid tetraether lipids: Implications for past sea surface temperature reconstructions. *Geochimica et Cosmochimica Acta*, 74(16), 4639–4654. <https://doi.org/10.1016/j.gca.2010.05.027>
- Lagabrielle, Y., Godderis, Y., Donadieu, Y., Malavieille, J., & Suarez, M. (2009). The tectonic history of Drake Passage and its possible impacts on global climate. *Earth and Planetary Science Letters*, 279(3–4), 197–211. <https://doi.org/10.1016/j.epsl.2008.12.037>
- Lazarus, D. B., Hollis, C. J., & Apel, M. (2008). Patterns of opal and radiolarian change in the Antarctic mid-Paleogene: Clues to the origin of the Southern Ocean. *Micropaleontology*, 54, 41–51.
- Lear, C. H., Bailey, T. R., Pearson, P. N., Coxall, H. K., & Rosenthal, Y. (2008). Cooling and ice growth across the Eocene–Oligocene transition. *Geology*, 36(3), 251–254. <https://doi.org/10.1130/G24584A.1>
- Liu, Z., Pagani, M., Zinniker, D., DeConto, R., Huber, M., Brinkhuis, H., et al. (2009). Global cooling during the Eocene–Oligocene climate transition. *Science*, 323(5918), 1187–1190. <https://doi.org/10.1126/science.1166368>
- Ludwig, W., Krasheninnikov, V., Basov, I., Bayer, U., Bloemendal, J., Bornhold, B., et al. (1980). Site 511. *Initial Reports of the Deep Sea Drilling Project*, 71, 21–109.
- Mallinson, D. J., Flower, B., Hine, A., Brooks, G., & Garza, R. M. (2003). Paleoclimate implications of high latitude precession-scale mineralogical fluctuations during early Oligocene Antarctic glaciation: The Great Australian Bight record. *Global and Planetary Change*, 39(3–4), 257–269. [https://doi.org/10.1016/S0921-8181\(03\)00119-X](https://doi.org/10.1016/S0921-8181(03)00119-X)
- Marret, F., & Zonneveld, K. A. F. (2003). Atlas of modern organic-walled dinoflagellate cyst distribution. *Review of Palaeobotany and Palynology*, 125(1–2), 1–200. [https://doi.org/10.1016/S0034-6667\(02\)00229-4](https://doi.org/10.1016/S0034-6667(02)00229-4)
- McGowran, B. (2009). The Australo-Antarctic Gulf and the Auversian facies shift. *Geological Society of America Special Papers*, 452, 215–240.
- Menden-Deuer, S., Lessard, E. J., Satterberg, J., & Grünbaum, D. (2005). Growth rates and starvation survival of three species of the pallium-feeding, thecate dinoflagellate genus *Protoperdinium*. *Aquatic Microbial Ecology*, 41(2), 145–152. <https://doi.org/10.3354/ame041145>

- Mohr, B. A. R. (1990). Eocene and Oligocene sporomorphs and dinoflagellate cysts from Leg 113 drill sites, Weddell Sea, Antarctica. In P. F. Barker, J. R. Kennett, et al. (Eds.), *Proceedings of the Ocean Drilling Program, Scientific Results 113* (pp. 595–612).
- Müller, P. J., Kirst, G., Ruhland, G., Von Storch, L., & Rosell-Melé, A. (1998). Calibration of the alkenone paleotemperature index $U^{K'}$ ₃₇ based on core-tops from the eastern South Atlantic and the global ocean. *Geochimica et Cosmochimica Acta*, 62(10), 1757–1772. [https://doi.org/10.1016/S0016-7037\(98\)00097-0](https://doi.org/10.1016/S0016-7037(98)00097-0)
- Nicol, S., Pauly, T., Bindoff, N. L., Wright, S., Thiele, D., Hosie, G. W., et al. (2000). Ocean circulation off East Antarctica affects ecosystem structure and sea-ice extent. *Nature*, 406(6795), 504–507. <https://doi.org/10.1038/35020053>
- Passchier, S., Bohaty, S. M., Jiménez-Espejo, F., Pross, J., Röhl, U., Van De Flierdt, T., et al. (2013). Early Eocene to middle Miocene cooling and aridification of East Antarctica. *Geochemistry, Geophysics, Geosystems*, 14, 1399–1410. <https://doi.org/10.1002/ggge.20106>
- Pearson, P. N., Foster, G. L., & Wade, B. S. (2009). Atmospheric carbon dioxide through the Eocene-Oligocene climate transition. *Nature*, 461(7267), 1110–1113. <https://doi.org/10.1038/nature08447>
- Peters, S. E., Carlson, A. E., Kelly, D. C., & Gingerich, P. D. (2010). Large-scale glaciation and deglaciation of Antarctica during the Late Eocene. *Geology*, 38(8), 723–726. <https://doi.org/10.1130/G31068.1>
- Prahl, F. G., & Wakeham, S. G. (1987). Calibration of unsaturation patterns in long-chain ketone compositions for palaeotemperature assessment. *Nature*, 330(6146), 367–369. <https://doi.org/10.1038/330367a0>
- Pross, J., Houben, A. J. P., van Simaëys, S., Williams, G. L., Kotthoff, U., Coccioni, R., et al. (2010). Umbria-Marche revisited: A refined magnetostratigraphic calibration of dinoflagellate cyst events for the Oligocene of the Western Tethys. *Review of Palaeobotany and Palynology*, 158(3–4), 213–235. <https://doi.org/10.1016/j.revpalbo.2009.09.002>
- Reichart, G., & Brinkhuis, H. (2003). Late Quaternary *Protoperidinium* cysts as indicators of paleoproductivity in the northern Arabian Sea. *Marine Micropaleontology*, 49(4), 303–315. [https://doi.org/10.1016/S0377-8398\(03\)00050-1](https://doi.org/10.1016/S0377-8398(03)00050-1)
- Roberts, A. P., Bicknell, S. J., Byatt, J., Bohaty, S. M., Florindo, F., & Harwood, D. M. (2003). Magnetostratigraphic calibration of Southern Ocean diatom datums from the Eocene–Oligocene of Kerguelen Plateau (Ocean Drilling Program Sites 744 and 748). *Palaeogeography, Palaeoclimatology, Palaeoecology*, 198(1–2), 145–168. [https://doi.org/10.1016/S0031-0182\(03\)00397-3](https://doi.org/10.1016/S0031-0182(03)00397-3)
- Röhl, U., Brinkhuis, H., Stickley, C. E., Fuller, M., Schellenberg, S. A., Wefer, G., & Williams, G. L. (2004). Sea level and astronomically induced environmental changes in Middle and Late Eocene sediments from the East Tasman Plateau. In N. F. Exon, J. P. Kennett, & M. J. Malone (Eds.), *The Cenozoic Southern Ocean: Tectonics, Sedimentation, and Climate Change Between Australia and Antarctica, Geophysical Monograph Series* (Vol. 151, pp. 127–151). Washington, DC: American Geophysical Union.
- Sangiorgi, F., van Soelen, E. E., Spofforth, D. J. A., Pälke, H., Stickley, C. E., St. John, K., et al. (2008). Cyclicity in the middle Eocene central Arctic Ocean sediment record: Orbital forcing and environmental response. *Paleoceanography*, 23, PA1S08. <https://doi.org/10.1029/2007PA001487>
- Scher, H. D., Bohaty, S. M., Smith, B. W., & Munn, G. H. (2014). Isotopic interrogation of a suspected late Eocene glaciation. *Paleoceanography and Paleoclimatology*, 29, 628–644. <https://doi.org/10.1002/2014PA002648>
- Scher, H. D., Bohaty, S. M., Zachos, J. C., & Delaney, M. L. (2011). Two-stepping into the icehouse: East Antarctic weathering during progressive ice-sheet expansion at the Eocene-Oligocene transition. *Geology*, 39(4), 383–386. <https://doi.org/10.1130/G31726.1>
- Scher, H. D., & Martin, E. E. (2006). Timing and climatic consequences of the opening of Drake Passage. *Science*, 312(5772), 428–430. <https://doi.org/10.1126/science.1120044>
- Schouten, S., Hopmans, E. C., Schefuss, E., & Sinninghe Damsté, J. S. (2002). Distributional variations in marine crenarchaeotal membrane lipids: A new tool for reconstructing ancient sea water temperatures? *Earth & Planetary Science Letters*, 204(1–2), 265–274. [https://doi.org/10.1016/S0012-821X\(02\)00979-2](https://doi.org/10.1016/S0012-821X(02)00979-2)
- Schouten, S., Huguët, C., Hopmans, E. C., Kienhuis, M. V., & Sinninghe Damsté, J. S. (2007). Analytical methodology for TEX₈₆ paleothermometry by high-performance liquid chromatography/atmospheric pressure chemical ionization-mass spectrometry. *Analytical Chemistry*, 79(7), 2940–2944. <https://doi.org/10.1021/ac062339v>
- Schumacher, S., & Lazarus, D. (2004). Regional differences in pelagic productivity in the late Eocene to early Oligocene—A comparison of southern high latitudes and lower latitudes. *Palaeogeography, Palaeoclimatology, Palaeoecology*, 214(3), 243–263. [https://doi.org/10.1016/S0031-0182\(04\)00424-9](https://doi.org/10.1016/S0031-0182(04)00424-9)
- Shafik, S., & Idnurm, M. (1997). Calcareous microplankton and polarity reversal stratigraphies of the Upper Eocene Browns Creek clay in the Otway Basin, Southeast Australia: Matching the evidence. *Australian Journal of Earth Sciences*, 44(1), 77–86. <https://doi.org/10.1080/08120099708728295>
- Sijp, W. P., Anna, S., Dijkstra, H. A., Flögel, S., Douglas, P. M., & Bijl, P. K. (2014). The role of ocean gateways on cooling climate on long time scales. *Global and Planetary Change*, 119, 1–22. <https://doi.org/10.1016/j.gloplacha.2014.04.004>
- Sijp, W. P., England, M. H., & Huber, M. (2011). Effect of the deepening of the Tasman Gateway on the global ocean. *Paleoceanography*, 26, PA4207. <https://doi.org/10.1029/2011PA002143>
- Sijp, W. P., von der Heydt, A. S., & Bijl, P. K. (2016). Model simulations of early westward flow across the Tasman Gateway during the early Eocene. *Climate of the Past*, 12(4), 807–817. <https://doi.org/10.5194/cp-12-807-2016>
- Sluijs, A., Bijl, P. K., Schouten, S., Röhl, U., Reichart, G. J., & Brinkhuis, H. (2011). Southern Ocean warming, sea level and hydrological change during the Paleocene-Eocene thermal maximum. *Climate of the Past*, 7(1), 47–61. <https://doi.org/10.5194/cp-7-47-2011>
- Sluijs, A., & Brinkhuis, H. (2009). A dynamic climate and ecosystem state during the Paleocene-Eocene thermal maximum: Inferences from dinoflagellate cyst assemblages on the New Jersey Shelf. *Biogeosciences*, 6(8), 1755–1781. <https://doi.org/10.5194/bg-6-1755-2009>
- Sluijs, A., Brinkhuis, H., Stickley, C. E., Warnaar, J., & Williams, G. L., Fuller, M. (2003). Dinoflagellate cysts from the Eocene-Oligocene transition in the Southern Ocean: Results from ODP Leg 189. *Proceedings of the Ocean Drilling Program, Scientific Results* 189.
- Sluijs, A., Pross, J., & Brinkhuis, H. (2005). From greenhouse to icehouse; organic-walled dinoflagellate cysts as paleoenvironmental indicators in the Paleogene. *Earth Science Reviews*, 68(3–4), 281–315. <https://doi.org/10.1016/j.earsci.2004.06.001>
- Stickley, C. E., Brinkhuis, H., McGonigal, K. L., Chaproniere, G. C. H., Fuller, M., Kelly, D. C., et al. (2004). Late Cretaceous–Quaternary biomagnetostratigraphy of ODP Sites 1168, 1170, 1171, and 1172, Tasmanian Gateway. *Proceedings of the Ocean Drilling Program, Scientific Results*, 189, 1–57.
- Stickley, C. E., Brinkhuis, H., Schellenberg, S. A., Sluijs, A., Rohl, U., Fuller, M., et al. (2004). Timing and nature of the deepening of the Tasmanian Gateway. *Paleoceanography*, 19, PA4027. <https://doi.org/10.1029/2004PA001022>
- Taylor, K. W. R., Huber, M., Hollis, C. J., Hernandez-Sanchez, M. T., & Pancost, R. D. (2013). Re-evaluating modern and Palaeogene GDGT distributions: Implications for SST reconstructions. *Global and Planetary Change*, 108, 158–174. <https://doi.org/10.1016/j.gloplacha.2013.06.011>

- Ternois, Y., Sicre, M. A., Boireau, A., & Conte, M. (1997). Evaluation of long-chain alkenones as paleo-temperature indicators in the Mediterranean Sea. *Deep Sea Research Part I: Oceanographic Research Papers*, *44*(2), 271–286. [https://doi.org/10.1016/S0967-0637\(97\)89915-3](https://doi.org/10.1016/S0967-0637(97)89915-3)
- Totterdell, J. M., Blevin, J. E., Struckmeyer, H. I. M., Bradshaw, B. E., Colwell, J. B., & Kennard, J. M. (2000). A new sequence framework for the Great Australian Bight: Starting with a clean slate. *The APPEA Journal*, *40*(1), 95–118. <https://doi.org/10.1071/AJ99007>
- Villa, G., Fioroni, C., Pea, L., Bohaty, S., & Persico, D. (2008). Middle Eocene–late Oligocene climate variability: Calcareous nannofossil response at Kerguelen Plateau, Site 748. *Marine Micropaleontology*, *69*(2), 173–192. <https://doi.org/10.1016/j.marmicro.2008.07.006>
- Vogt, P. R., & Conolly, J. R. (1971). Tasmantid Guyots, the age of the Tasman Basin, and motion between the Australia plate and the mantle. *Geological Society of America Bulletin*, *82*(9), 2577–2584. [https://doi.org/10.1130/0016-7606\(1971\)82\[2577:TGTAOT\]2.0.CO;2](https://doi.org/10.1130/0016-7606(1971)82[2577:TGTAOT]2.0.CO;2)
- Wade, B. S., Houben, A. J. P., Quaijtaal, W., Schouten, S., Rosenthal, Y., Miller, K. G., et al. (2012). Multiproxy record of abrupt sea-surface cooling across the Eocene–Oligocene transition in the Gulf of Mexico. *Geology*, *40*(2), 159–162. <https://doi.org/10.1130/G32577.1>
- Wade, B. S., Pearson, P. N., Berggren, W. A., & Pälike, H. (2011). Review and revision of Cenozoic tropical planktonic foraminiferal biostratigraphy and calibration to the geomagnetic polarity and astronomical time scale. *Earth-Science Reviews*, *104*(1–3), 111–142. <https://doi.org/10.1016/j.earscirev.2010.09.003>
- Warny, S., Kymes, C. M., Askin, R., Krajewski, K. P., & Tatur, A. (2018). Terrestrial and marine floral response to latest Eocene and Oligocene events on the Antarctic Peninsula. *Palynology*, 1–13. <https://doi.org/10.1080/01916122.2018.1477850>
- Wei, W., & Wise, S. W. (1990). Biogeographic gradients of middle Eocene–Oligocene calcareous nannoplankton in the South Atlantic Ocean. *Palaeogeography, Palaeoclimatology, Palaeoecology*, *79*(1–2), 29–61. [https://doi.org/10.1016/0031-0182\(90\)90104-F](https://doi.org/10.1016/0031-0182(90)90104-F)
- Weijers, J. W. H., Lim, K. L. H., Aquilina, A., Sinninghe Damsté, J. S. S., & Pancost, R. D. (2011). Biogeochemical controls on glycerol dialkyl glycerol tetraether lipid distributions in sediments characterized by diffusive methane flux. *Geochemistry, Geophysics, Geosystems*, *12*, Q10010. <https://doi.org/10.1029/2011GC003724>
- Weijers, J. W. H., Schouten, S., Spaargaren, O. C., & Sinninghe Damsté, J. S. (2006). Occurrence and distribution of tetraether membrane lipids in soils: Implications for the use of the TEX₈₆ proxy and the BIT index. *Organic Geochemistry*, *37*(12), 1680–1693. <https://doi.org/10.1016/j.orggeochem.2006.07.018>
- Williams, G. L., Brinkhuis, H. M. A. P., Pearce, M. A., Fensome, R. A., & Weegink, J. W. (2004). Southern Ocean and global dinoflagellate cyst events compared: Index events for the Late Cretaceous–Neogene. *Proceedings of the Ocean Drilling Program, Scientific Results*, *189*, 1–98.
- Williams, G. L., Fensome, R. A., & MacRae, R. A. (2017). *The Lentini and Williams index of fossil dinoflagellates 2017 edition* (p. 972). AASP Contributions Series 48.
- Williams, S. E., Whittaker, J. M., Halpin, J. A., & Müller, R. D. (2019). Australian–Antarctic breakup and seafloor spreading: Balancing geological and geophysical constraints. *Earth-Science Reviews*, *188*, 41–58. <https://doi.org/10.1016/j.earscirev.2018.10.011>
- Wise, S. W. (1983). Mesozoic and Cenozoic calcareous Nannofossils recovered by Deep Sea Drilling Project Leg 71 in the Falkland Plateau Region, Southwest Atlantic Ocean. In: Ludwig, W.J., Krashennikov, V.A., et al. *Initial Reports of the DSDP*, *71*, 481–550.
- Wrenn, J. H., & Hart, G. F. (1988). Paleogene dinoflagellate cyst biostratigraphy of Seymour Island. *Geological Society of America*, *169*, 321–447. <https://doi.org/10.1130/MEM169-p321>
- Wright, N. M., Scher, H. D., Seton, M., Huck, C. E., & Duggan, B. D. (2018). No change in Southern Ocean circulation in the Indian Ocean from the Eocene through late Oligocene. *Paleoceanography and Paleoclimatology*, *33*, 152–167. <https://doi.org/10.1002/2017PA003238>
- Zachos, J. C., Dickens, G. R., & Zeebe, R. E. (2008). An early Cenozoic perspective on greenhouse warming and carbon-cycle dynamics. *Nature*, *451*(7176), 279–283. <https://doi.org/10.1038/nature06588>
- Zhang, Y. G., Zhang, C. L., Liu, X.-L., Li, L., Hinrichs, K.-U., & Noakes, J. E. (2011). Methane index: A tetraether archaeal lipid biomarker indicator for detecting the instability of marine gas hydrates. *Earth and Planetary Science Letters*, *307*(3–4), 525–534. <https://doi.org/10.1016/j.epsl.2011.05.031>
- Zonneveld, K. A. F., Marret, F., Versteegh, G. J. M., Bogus, K., Bonnet, S., Bouimetarhan, I., et al. (2013). Atlas of modern dinoflagellate cyst distribution based on 2405 data points. *Review of Palaeobotany and Palynology*, *191*, 1–197. <https://doi.org/10.1016/j.revpalbo.2012.08.003>